Applied Energy 401 (2025) 126805

Contents lists available at ScienceDirect

Applied Energy

journal homepage: www.elsevier.com/locate/apenergy

Long-term impacts and design considerations of dual-purpose wave farms for energy generation and coastal protection

Avinash Boodoo [a,*], Jeffrey S. Cross [a], Christopher Ridgewell [b], Ville Kortelainen [b], Matti Vuorinen [b], Amina Harouna-Mayer [b]

[a] Department of Transdisciplinary Science and Engineering, School of Environment and Society, Institute of Science Tokyo, 152-8550, Japan
[b] AW-Energy Oy, Tikkurilantie 10, FI-01380 Vantaa, Finland

HIGHLIGHTS

- First long-term study of dual-use wave farms for energy and coastal protection.
- Wave farm retained 278,427 m^3 of sediment over 20 years, reducing erosion by 42 %.
- Annual output of 562.3 MWh per device with 49.9 % capture efficiency.
- Wave attenuation peaked during low-energy conditions, offering year-round protection.
- Tighter spacing enhances protection; greater distance offshore increases energy output.

GRAPHICAL ABSTRACT

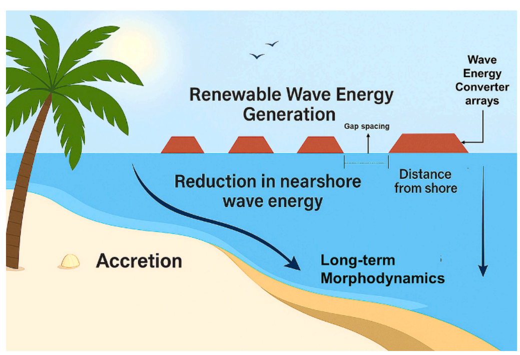

ARTICLE INFO

Keywords:
Wave energy converters
Wave farms
Coastal protection
Morphodynamics
Renewable energy
Wave energy

ABSTRACT

The dual use of wave farms for renewable energy generation and coastal protection presents a promising strategy to reduce the Levelized Cost of Electricity (LCoE) and improve the economic feasibility of wave energy. However, no prior study has quantified the long-term morphodynamic impacts of wave farms or evaluated how seasonal wave conditions influence energy output and coastal protection effectiveness. This study presents the first integrated assessment of a nearshore WaveRoller Wave Energy Converter (WEC) array over 1-, 10-, and 20-year periods, using a field-validated, coupled depth-averaged (2DH) hydrodynamic, spectral wave, and sediment transport model in Delft3D. Nine deployment configurations were simulated to explore how array layout (spacing and distance from shore) affects wave attenuation, sediment retention, and energy output. Results show that the WaveRoller array produced 562.3 MWh annually per device, with a capacity factor of 18.34 % and a capture efficiency of 49.9 %. The system also retained up to 278,427 m^3 of sediment after 20 years, with a sediment retention per unit area of 1.941 m^3/m^2. Wave attenuation was greatest during low-to-moderate energy conditions, suggesting year-round protection benefits. Sensitivity analyses revealed a trade-off between energy yield and erosion mitigation, with tighter spacing enhancing sediment retention and moderate distances offshore improving energy yield. By quantifying energy production and erosion mitigation under different design scenarios, this study demonstrates the dual functionality of wave farms and supports their use as multi-functional

* Corresponding author.
E-mail address: boodoo.a.aa@m.titech.ac.jp (A. Boodoo).

https://doi.org/10.1016/j.apenergy.2025.126805
Received 20 June 2025; Received in revised form 19 July 2025; Accepted 17 September 2025
Available online 25 September 2025

coastal infrastructure. These results offer a foundation for future techno-economic models that incorporate both energy and coastal protection outcomes.

1. Introduction

Wave energy is a promising renewable resource with the potential to meet growing global energy demands while contributing to carbon-free energy generation [7,8,12,24,28,35,38]. The estimated global wave energy resources lie in the range of 1–10 TW [19,23,24] with estimates of global annual wave power in the range of 29,500 and 32,000 TW h/year [7,24,28] which exceeded the global annual energy consumption in 2018 of 26,700 TW h/year [28].

While wave energy surpasses other traditional renewable energy sources in several aspects including its high availability (up to 90 %); the highest energy density among all the renewables and minimal negative impacts on the environment [5,24,31,44,45], the high capital costs and Levelized Cost of Electricity (LCoE) of wave energy currently hinder its competitiveness with established renewables like solar and wind, as well as fossil fuels, limiting widespread development and implementation [8,18,21,24,35,46,50].

A promising strategy to offset these economic challenges is the dual use of wave farms for both energy generation and coastal protection. By replacing conventional coastal protection structures such as breakwaters with wave energy converters (WECs), wave farms can attenuate wave energy and mitigate coastal erosion while simultaneously generating renewable energy [1,2,11,13,17,21,33,40]. This multi-functional approach is particularly relevant in the context of climate change and sea level rise (SLR), where traditional coastal protection structures may become increasingly ineffective. Although several studies have examined the effectiveness of wave farms for coastal protection, significant knowledge gaps remain.

While previous studies [1–4,9,40,42,43] have demonstrated the short-term (days to weeks) effectiveness of wave farms in reducing wave energy and mitigating erosion, particularly during storm events, their long-term impact on coastal morphodynamics and energy production has never been explored. No study has assessed how wave farms influence morphodynamics and trends of erosion and accretion over timescales of months to decades (1 year, 10 years, 20 years), nor has any research examined the effects of seasonal wave variability on energy output and morphodynamics. Understanding these long-term effects is essential for evaluating the viability of wave farms as a long-term sustainable solution for coastal protection and renewable energy generation.

Moreover, the long-term contribution of wave farms to coastal protection, specifically in terms of erosion mitigation has yet to be quantified. The estimation of the volume of sediment retained through erosion mitigation over long-term periods can provide essential data for techno-economic assessments, enabling the integration of coastal protection benefits into economic evaluations. By accounting for the reduced need for conventional coastal protection structures, this approach can contribute to lowering the high Levelized Cost of Energy (LCoE) and enhancing the overall competitiveness of wave energy [14].

While some studies have analyzed the effects of inter-device spacing [16,17,41–43] and the distance from the coast [4,26] on coastal protection, no research has explored how these factors collectively influence the optimal balance between maximizing coastal protection and maintaining efficient energy generation. Understanding this relationship is critical for designing wave farms that effectively mitigate coastal erosion while ensuring sufficient wave energy extraction to ensure economic feasibility and long-term sustainability. Addressing these gaps is crucial for optimizing wave farm configurations and establishing their viability as a long-term dual-purpose solution for renewable energy generation and coastal protection.

To address these gaps, this study presents the first long-term, field-validated numerical modelling assessment of a dual-purpose wave farm. The specific objectives of this study are: (i) to assess the influence of seasonal wave conditions on energy output and coastal protection through wave attenuation, (ii) to investigate the long-term impacts of wave farms on coastal morphodynamics and to quantify their effectiveness in mitigating cumulative erosion across short-, medium-, and long-term timescales and (iii) to examine how key design parameters, including gap spacing and distance from shore, influence the balance between long-term coastal protection and energy generation efficiency.

This study employs a numerical modelling approach using a coupled depth-averaged (2DH) hydrodynamic, spectral wave, and sediment transport model in Delft3D. The WaveRoller WEC, developed by AW-Energy, is used in this study and the model is calibrated and validated using field data collected from Almagreira Beach, Portugal, where AW-Energy previously deployed and tested the device. The WaveRoller is a bottom-hinged oscillating surge WEC designed to operate in shallow water, making it particularly suitable for modifying nearshore wave conditions and influencing sediment transport. Its ability to both extract energy and affect wave propagation in the coastal zone makes it a promising candidate for dual-use applications involving coastal protection and renewable energy generation.

Almagreira Beach, situated along Portugal's western coast, was selected as the study site due to its highly energetic wave climate, making it well-suited for wave energy extraction. Its history as a WaveRoller testing site provides access to extensive wave and environmental data, enabling robust model calibration and validation. Additionally, the site's dynamic coastal morphology, characterized by a sandy shoreline and moderate tidal range, makes it an ideal location for investigating the long-term influence of wave farms on sediment transport and morphodynamics.

This paper is structured as follows: Section 2 presents the study area characteristics, numerical modelling setup, and data analysis techniques. Section 3 details the results, focusing on wave attenuation, morphodynamic changes and energy production trends. Section 4 provides a discussion of results, highlighting key findings and study limitations, and Section 5 concludes with potential applications and future research directions.

2. Methodology

2.1. Study site

The area under study, Almagreira Beach, is located between 39°22′30"N and 39°24′15"N latitude and 9°17′25"W and 9°19′50"W longitude, extending from the shoreline to a water depth of approximately 25 m (Fig. 1). Almagreira Beach is characterized as a high-energy, dissipative sandy beach, influenced by energetic Atlantic swells and active sediment transport processes. It faces northwest and is fully exposed to dominant swell directions, making it a representative site for wave energy investigations and morphodynamic studies [20,27].

The wave climate at Almagreira Beach is dominated by North Atlantic swells, with significant wave heights (H_{sig}) typically ranging from 2 to 3 m in winter and 1 to 2 m in summer, and peak wave periods (T_p) between 8 and 14 s [20,27,39]. The dominant wave direction is from the northwest and shows little seasonal variation, as the mean direction (D_m) remains practically unchanged throughout the year. Higher-energy conditions prevail from October to March, while summer months are generally calmer [27]. Extreme storm events with H_{sig} exceeding 4.5 m typically occur 4 to 8 times per year, with most extreme wave heights ranging between 5 and 7 m, and occasionally exceeding 7 m [20,27,39]. The average annual H_{sig} is approximately 2.2 m, corresponding to a mean wave power of 18.64 kW/m. Seasonal wave power ranges from 10.62 kW/m in summer to 27.58 kW/m in winter, with peak values exceeding 100 kW/m during storm events [27].

The beach is subject to a semi-diurnal tidal regime, with tidal ranges varying from approximately 1 m during neap tides to 3 m during spring tides [27,39]. While tidal currents have minimal influence on nearshore flow patterns, the tidal cycle plays an important role in modulating nearshore hydrodynamics by affecting wave breaking patterns and sediment transport. The beach profile is gently sloping, with a wide surf zone characteristic of dissipative beach environments [27] as seen in Fig. 1B.

Sediment transport at Almagreira is highly active due to the energetic wave climate. The estimated annual volume of transported sediment is on the order of 10^6 m^3/year [27]. The beach exhibits both seasonal and event-driven patterns of erosion and accretion, consistent with storm-driven morphological change observed in similar high-energy beach environments. The closure depth, below which no significant morphological changes occur, is approximately 12 to 14 m [27]. The median grain size (D_{50}) of bottom sediments typically ranges from 0.2 to 0.5 mm, corresponding to medium sands, with slight spatial variability across the profile [39].

Almagreira Beach served as the pilot site for the WaveRoller device developed by AW-Energy. The WEC was deployed in 2009 at a water depth of approximately 12 m, within the active morphodynamic zone and near the closure depth of the beach profile [27]. This positioning is particularly relevant to the present study, which aims to assess the long-term impacts of wave farms, represented numerically by arrays of multiple WaveRoller devices, on coastal morphodynamics and sediment transport. While only one device was physically deployed, the numerical modelling framework extends this to examine cumulative effects from a wave farm configuration, allowing for a more comprehensive evaluation of potential morphological and hydrodynamic changes. The availability of detailed wave, sediment, and morphological datasets from this deployment provides a strong foundation for assessing the long-term influence of wave farms on coastal processes.

2.2. Numerical modelling approach

2.2.1. Model description

A process-based, depth-averaged (2DH) numerical model was developed using Delft3D to simulate coupled hydrodynamics, spectral wave transformation, sediment transport, and long-term morphological change at Almagreira Beach. The use of a 2DH modelling approach was chosen for the nearshore conditions at Almagreira Beach, where the deployment depth (~12 m) lies within the active morphodynamic zone and is strongly influenced by wave-driven processes. In such environments, vertical stratification is typically limited, and depth-averaged models provide a practical compromise between representing key nearshore dynamics and ensuring computational efficiency. This approach enables the simulation of long-term morphological evolution

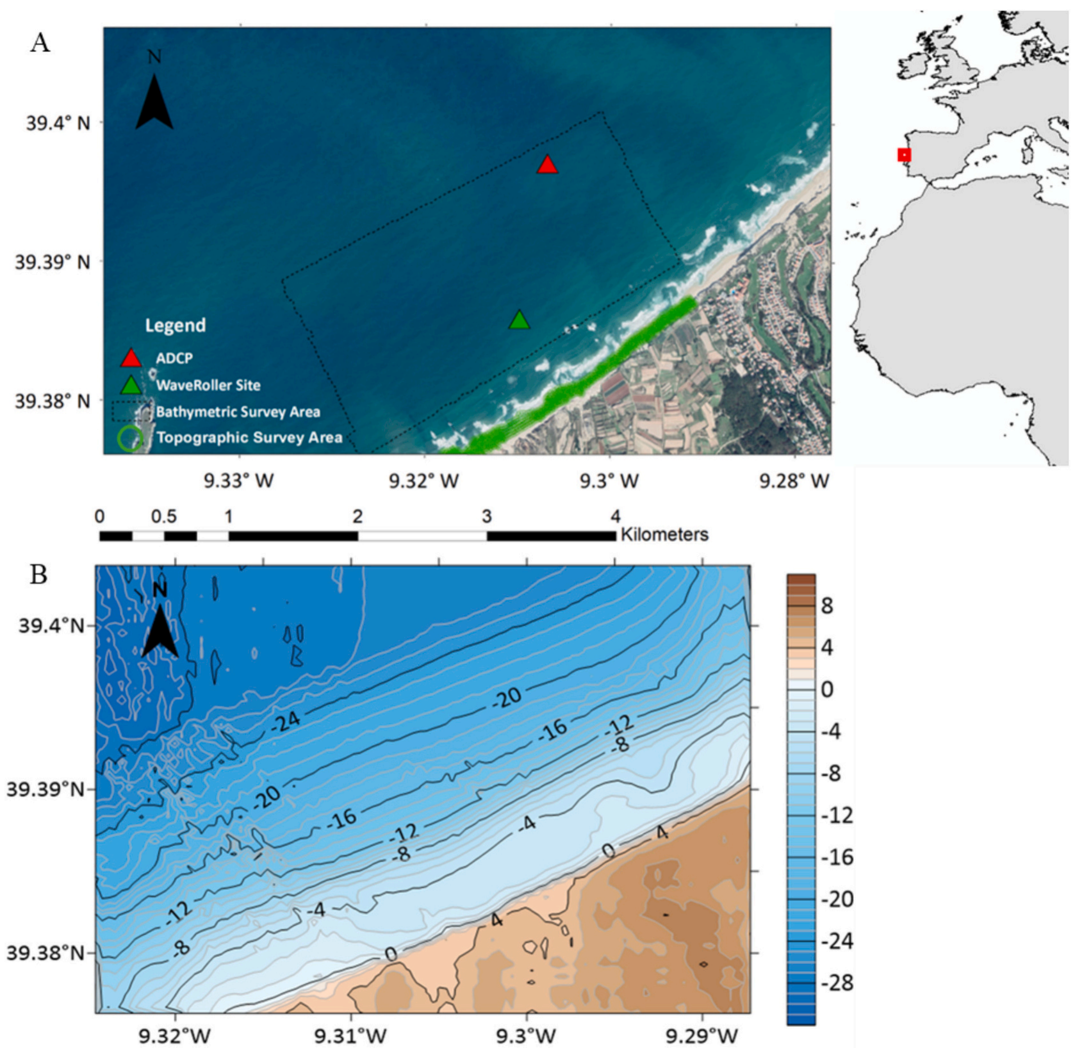

Fig. 1. (A) Location of study area, nearshore ADCP, historical WaveRoller testing site and topographic survey area, (B) Bathymetry of Almagreira Beach.

over multi-year and decadal time scales, which would be computationally expensive with fully 3D models. Given the study's focus on large-scale morphodynamic changes rather than vertical flow structure, the 2DH model is considered appropriate and sufficient for the objectives of this research. The model consists of three dynamically linked components: Delft3D-FLOW (hydrodynamics), Delft3D-WAVE (SWAN), and the Morphology module.

An online coupling was implemented between Delft-FLOW and Delft-WAVE, enabling two-way interaction at each computational timestep. The wave module simulates the propagation of random, short-crested wind waves in coastal areas, accounting for depth-induced breaking, bottom friction, and wave–current interaction. Radiation stress gradients computed in the wave module are passed to the hydrodynamic model to influence flow patterns and sediment mobility. Conversely, time-varying water levels and flow velocities from the FLOW module are used to update wave propagation and energy dissipation in Delft-WAVE. The Morphology module was activated to simulate bathymetric changes driven by both wave- and current-induced sediment transport.

2.2.1.1. Hydrodynamic model. The hydrodynamic model, Delft3D-FLOW, solves the unsteady Shallow Water Equations (SWE), which include the horizontal momentum and continuity equations, using a finite difference scheme on a structured grid [29]. The model is forced at open boundaries by tidal and meteorological inputs and is widely used to simulate flow dynamics in coastal and shallow marine environments. It computes depth-averaged flow velocities and water level variations in response to tidal forcing, pressure gradients, and bed friction. Delft3D-FLOW is particularly well suited for resolving nearshore current patterns that influence sediment transport, and in this study, it provides the hydrodynamic foundation for the coupled modelling of long-term morphodynamic change.

2.2.1.2. Spectral wave model. The spectral wave module, Delft3D-WAVE, is based on the SWAN (Simulating WAves Nearshore) model, which solves the spectral action balance equation (Eq. 1) to simulate the propagation and transformation of random, short-crested wind waves in coastal and nearshore environments. It accounts for processes including wave generation by wind, whitecapping, depth-induced breaking, bottom friction, shoaling, refraction, and nonlinear wave–wave interactions.

$$\frac{\partial N}{\partial t}+\nabla_{\vec{x}}\cdot\left[\left(\vec{c_g}+\vec{u}\nabla\right)N\right]+\frac{\partial c_\sigma N}{\partial \sigma}+\frac{\partial c_\theta N}{\partial \theta}=\frac{S_{tot}}{\sigma} \quad (1)$$

This equation governs the evolution of wave action density $N(\sigma,\theta)$ in time, space, frequency, and direction. The first term represents the local rate of change of wave action; the second term captures spatial propagation driven by wave group velocity $\vec{c_g}$ and ambient currents $\vec{u}$. The third and fourth terms represent shifts in frequency and direction due to shoaling and refraction. The right-hand side, $\frac{S_{tot}}{\sigma}$, represents the net source term, incorporating wind input, whitecapping, bottom friction, depth-induced breaking, and nonlinear interactions. Model inputs include bathymetric data, wave and wind data. Key physical processes such as whitecapping, bottom friction, and wave breaking were activated. WECs are represented in the model as partial obstacles with specific reflection (K_r) and transmission (K_t) coefficients [14].

2.2.1.3. Morphodynamic model. The morphodynamic component of the model was implemented using the Morphology module within Delft3D-FLOW. This module computes bed level changes over time by solving the sediment continuity equation, which accounts for gradients in sediment transport induced by hydrodynamic and wave forcing. Sediment transport is calculated using the Van Rijn formulation, which includes both bedload and suspended load under combined wave-current interactions.

The model was run in depth-averaged (2DH) mode, and morphological updates were applied at each hydrodynamic time step using the Exner equation:

$$\frac{\partial z_b}{\partial t}+\frac{1}{1-p}\nabla\cdot\vec{q_s}=0 \quad (2)$$

Where z_b is the bed level elevation, p is the sediment porosity, and $\vec{q_s}$ is the total sediment transport vector (bedload + suspended load). To simulate long-term seabed evolution efficiently, a morphological scale factor (morfac) is applied, which scales up the rate of bed level change relative to hydrodynamic time. This technique allowed for the simulation of decadal scale morphodynamic trends over shorter computational periods and is widely used in studies of coastal evolution. The Morphology module is essential for assessing shoreline evolution, spatial patterns of sediment deposition and erosion, and the long-term coastal response to the presence of WECs.

2.3. Model set-up

The coupled 2DH hydrodynamic, spectral wave, and morphodynamic model was developed in Delft3D to simulate long-term sediment transport and wave energy transformation at Almagreira Beach, Portugal. The model setup involved generating a structured grid, interpolating high-resolution site-specific bathymetric and topographic survey data, and incorporating tidal, wave, wind, and sediment boundary conditions derived from a combination of observational and reanalysis datasets.

The spectral wave model (Delft3D-WAVE) was implemented using a two-level nested grid configuration to simulate wave transformation from offshore to the nearshore region (Fig. 2). The outer wave grid, covering an area of 3 km × 3 km, was forced at the northwestern boundary using hourly ERA5 reanalysis data from 29 October 2009 to 29 October 2010, including H_{sig}, T_P, and D_m. ERA5 10 m wind data consisting of wind speed and direction was also applied uniformly across the domain to account for wind-wave interactions. ERA Reanalysis data has been used in previous numerical modelling studies [30,36,45,17] to evaluate the energy production and has been proven reliable.

The outer wave grid supplied boundary conditions to a high-resolution nested inner grid covering the area around the WaveRoller deployment site. This inner grid matched the hydrodynamic model (Delft3D-FLOW) domain in both extent and resolution (2.8 km × 1.5 km, with grid cells of 25 m × 12.5 m) and was discretized into a structured grid of 157 × 37 cells, totalling 5809 elements. High-resolution bathymetric and topographic data, collected for the WaveRoller deployment using single-beam echo sounding and GPS-based surveys, were

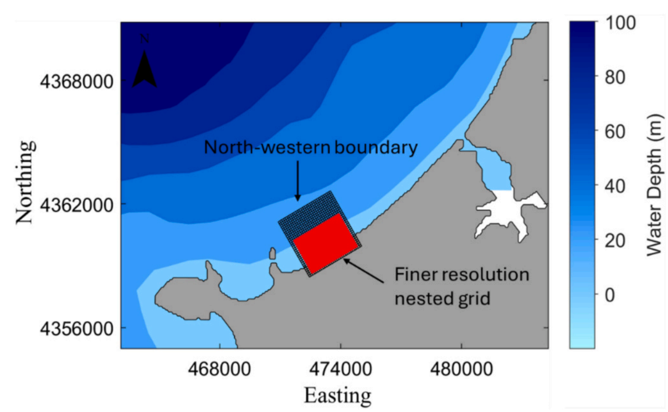

Fig. 2. Nested Delft3D-WAVE Model Domain and Bathymetry at Almagreira Beach, Portugal. The outer grid (black) represents the coarse-resolution model domain forced with ERA5 wave data at the northwestern boundary. The inner red grid shows the finer-resolution nested domain used to resolve nearshore wave transformation and interactions with the WaveRoller array. (For interpretation of the references to colour in this figure legend, the reader is referred to the web version of this article.)

interpolated onto the inner model grid.

The WaveRoller array was represented in the inner wave grid as partially reflective obstacles using transmission (K_t) and reflection (K_r) coefficients to simulate localized wave energy dissipation. These values were selected to approximate the hydrodynamic behaviour of the device as a bottom-hinged, nearshore, surge-type structure that interacts strongly with incoming waves. Previous numerical modelling studies [1,2,4,9–11] have used reported values from the WaveCat WEC with K_t = 0.76 and K_r = 0.43. However, there are no reported values for a WaveRoller-type device, whose physical configuration resembles a reflective vertical barrier and whose nearshore deployment leads to significant wave obstruction. This justifies the use of higher reflection and lower transmission values, consistent with those reported for vertical impermeable breakwaters, which typically exhibit reflection coefficients between 0.7 and 0.9 and transmission coefficients between 0.1 and 0.3 [22,32]. Furthermore, a recent systematic review of wave farm modelling studies by Boodoo, Wakeyama, and Cross [13] found that reflection coefficients in the range of 0.5–0.9 and transmission coefficients of 0.1–0.5 are commonly used in similar studies.

While reflection and transmission coefficients can vary with wave frequency and angle of incidence, Delft3D-WAVE (based on the standard SWAN implementation) does not support frequency-dependent K_t and reflection K_r values. Therefore, constant coefficients were used to approximate the average behaviour of the WECs across the modelled sea state conditions. Delft3D-WAVE does not simulate energy absorption explicitly. The wave field is modified based on the specified K_t and K_r, and any residual energy not reflected or transmitted is removed from the spectrum as a simplified representation of WEC-induced effects. This removed energy is not directly linked to device power capture. Unlike models such as SNL-SWAN, which allow frequency-dependent energy absorption, our framework treats wave transformation and energy extraction as decoupled processes. This approach has been widely adopted in studies investigating the coastal protection effectiveness of wave farms [1,2,4,10,11,40,14].

A linear array of 10 devices, each 12.5 m wide, was positioned perpendicular to the shoreline in approximately 12 m water depth (approximately 600 m offshore), with a 2D (25 m) gap spacing between devices (Fig. 3). Open boundary conditions were applied at the northwestern edge of the hydrodynamic model domain, where tidal forcing was imposed using 14 harmonic constituents (A0, M2, S2, N2, K2, K1, O1, P1, Q1, MF, MM, M4, MS4, MN4) derived from the TPXO7.2 global tidal model. Neumann boundary conditions were applied at the lateral boundaries. The same ERA5 10 m wind data used in the wave model was also applied in FLOW for consistency.

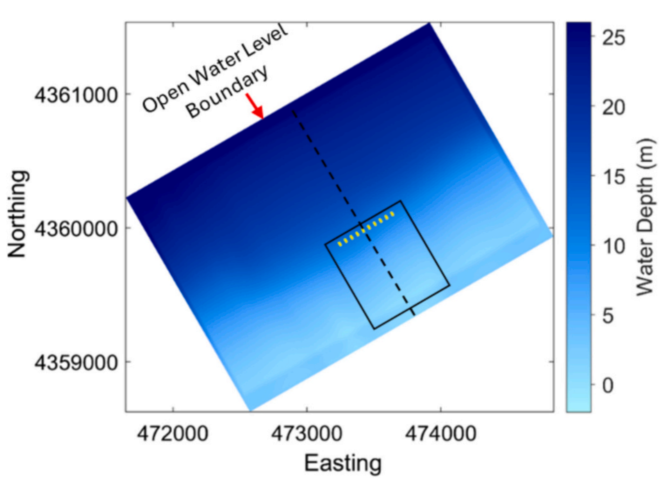

Fig. 3. Model domain used for both Delft3D-FLOW and Delft3D-WAVE simulations at Almagreira Beach, Portugal. The open water level boundary is indicated by the red arrow, and the yellow dots represent the WaveRoller array positioned at approximately 12 m depth. The black box delineates the control zone used for wave attenuation and morphodynamic analyses, while the black dashed line indicates the cross-shore transect used for bed level validation. (For interpretation of the references to colour in this figure legend, the reader is referred to the web version of this article.)

Sediment transport was modelled using the van Rijn [47] formulation with a D_{50} of 200 μm, a specific density of 2650 kg/m^3, and a dry bed density of 1600 kg/m^3. The final sediment transport calibration factors applied in all simulations were 0.3 for wave-related suspended and bedload transport, and 0.3 for current-related transport magnitude. These values were selected following calibration and validation (see Section 2.2.6). A summary of the model parameters is shown in Table 1. The coupled model was first run without WECs to establish a baseline scenario for calibration and validation. Following this, the WaveRoller array was introduced, and simulations were conducted for a one-year period (29 October 2009–29 October 2010).

To simulate long-term morphodynamic evolution, a morfac was applied. In Delft3D, the morfac scales the computed bed level change per hydrodynamic time step, enabling long-term seabed evolution to be simulated over a shorter physical period. In this study, morfac values of 1, 10, and 20 were used to represent 1-year, 10-year, and 20-year morphodynamic scenarios, respectively. This approach assumes that the one-year wave and hydrodynamic forcing period is representative of long-term average conditions. A control zone was defined within the nearshore region behind the WaveRoller array to facilitate consistent spatial analysis of wave attenuation, sediment retention, and morphological changes. This zone, shown in Fig. 3, was used throughout the study for extracting comparative metrics between baseline and WEC scenarios.

Table 1
Key Parameters Used in the Coupled Delft3D Wave, Flow, and Morphodynamic Simulations

Parameter	Value
Wave Model (Delft3D-WAVE)	
Outer grid extent	3 km × 3 km
Inner grid extent	2.8 km × 1.5 km
Inner grid resolution	25 m × 12.5 m
Grid Cells	157 × 37 (5809 total)
Offshore wave forcing	ERA5 (hourly Hsig, Tp, Dm)
Wind forcing	ERA5 hourly wind data 10 m (wind speed, wind direction)
Transmission coefficient (WECs)	0.2
Reflection coefficient (WECs)	0.8
Simulation period	29 Oct 2009–29 Oct 2010
Hydrodynamic Model (Delft3D-FLOW)	
Domain extent	2.8 km × 1.5 km
Grid cells	157 × 37 (5809 total)
Tidal boundary forcing	14 constituents (TPXO7.2)
Open Boundary	Northwestern Boundary
Lateral boundaries	Neumann boundary conditions
Wind forcing	ERA5 hourly wind data 10 m (wind speed, wind direction)
Sediment Properties	
Median sediment diameter (D_{50})	200 μm
Specific density	2650 kg/m^3
Morphodynamic Settings	
Sediment transport formulation	[47]
Morphological scale factor (morfac)	1, 10, 20
Wave-related suspended transport factor	0.3
Wave-related bedload transport factor	0.3
Current-related transport vector magnitude	0.3
Current-related reference concentration factor	0.3

2.3.1. Model calibration and validation

The coupled hydrodynamic, spectral wave, and sediment transport model was calibrated and validated using field data collected at Almagreira Beach. The model was initially run without the WaveRoller array to establish a baseline scenario representing natural conditions. The H_{sig} and water levels were calibrated and validated using wave and current data from a nearshore 600 kHz RDI WORKHORSE Acoustic Doppler Current Profiler (ADCP) deployed at approximately 27 m water depth (Fig. 1), which recorded hourly measurements of H_{sig}, T_P, and D_m and water depth. Calibration of H_{sig} was carried out over the period from 29 October 2009 at 13:00 to 09 March 2010 at 11:40, during which wave breaking parameters, wind drag coefficients, and bottom friction factors were adjusted to improve agreement between modelled and observed wave conditions. Validation was conducted over the period from 01 June 2010 at 18:00 to 29 October 2010 at 11:00.

Water level validation was also performed using ADCP depth data. A one-month window (October 2010) was selected to assess the model's ability to reproduce spring–neap tidal variability. This allowed targeted evaluation of tidal dynamics using a hydrodynamically consistent time window and ensured direct comparison between modelled and observed water levels.

Morphodynamic validation was based on bathymetric and topographic survey data collected on 28 June 2010, which included a cross-shore transect near the WaveRoller deployment site (Fig. 3). In addition to the default sediment and morphodynamic parameters described in Section 2.2, transport factors for wave- and current-induced bedload and suspended load transport were initially set to 0.5 and were varied during calibration to optimize morphodynamic performance. Modelled bed level changes were compared to measured profiles to assess performance in reproducing erosion and accretion patterns.

Model performance was assessed by comparing simulated and observed time series of wave parameters and measured versus predicted bed levels. Quantitative performance metrics included the Root Mean Square Error (RMSE), Bias, Scatter Index (SI), Coefficient of Determination (R^2), and Skill Score. These performance metrics are widely used in coastal numerical modelling studies to assess model accuracy, and their definitions can be found in previous literature [2,11,13] for brevity, they are not described here.

2.4. Wave attenuation and Morphodynamic impact metrics

This study adopts an area-based approach to evaluate wave attenuation and sediment retention, computing spatial statistics across a fixed control zone rather than relying solely on cross-shore transects or representative points. This method enables a more robust and transferable assessment of the spatial extent and variability of wave farm impacts and represents a novel contribution to wave energy–coastal protection impact analysis. To evaluate the coastal protection effectiveness of the WEC array, a set of wave and morphodynamic metrics were computed. These include wave attenuation; wave energy flux reduction; percentage erosion reduction; total volume of sediment retained and sediment retention per unit area.

2.4.1. Wave attenuation

Wave attenuation was evaluated by comparing H_{sig} values from the baseline (no-WEC) and WEC scenarios within a fixed nearshore control zone located directly landward of the WEC array (Fig. 3). This zone, covering approximately 143,437.5 m^2, was selected to include the area most affected by wave transformation due to the WECs, and remained consistent across all scenarios to support direct comparison. Attenuation was calculated point-by-point at each grid cell by comparing wave heights in the WEC scenario to the baseline. Compared to single-point or transect-based methods, this area-based approach allows for a more comprehensive assessment of both the magnitude and spatial variability of wave attenuation across the full nearshore region of interest. It is particularly useful for identifying how wave reduction effects are distributed over space, which is important for understanding and evaluating the coastal protection potential of WEC arrays. The percentage reduction in H_{sig} at each grid point i was computed using Eq. 3:

$$A_i^H = \left(\frac{H_{\text{sig,noWEC},i} - H_{\text{sig,WEC},i}}{H_{\text{sig,noWEC},i}}\right) \times 100 \tag{3}$$

where A_i^H is the wave height attenuation (%) at grid point i, $H_{\text{sig,noWEC},i}$ is the H_{sig} at point i without WECs and $H_{\text{sig,WEC},i}$ is the H_{sig} at point i with WECs.

Statistical metrics including the mean, 75th percentile, maximum attenuation, standard deviation, and the percentage of grid points exceeding 10 % attenuation were computed to characterize spatial patterns and variability.

In addition, wave energy flux (i.e., wave power per unit crest width, in W/m) was obtained directly from the Delft3D-WAVE model outputs. This parameter provides a physically meaningful measure of the rate at which wave energy is transmitted toward the coast and is especially relevant for assessing the potential for erosion and sediment transport. The wave power attenuation at each grid point i was calculated as:

$$A_i^P = \left(\frac{P_{\text{noWEC},i} - P_{\text{WEC},i}}{P_{\text{noWEC},i}}\right) \times 100 \tag{4}$$

where A_i^P is the wave energy flux attenuation (%) at grid point i, $P_{\text{noWEC},i}$ is the wave energy flux at point i without WECs and $P_{\text{WEC},i}$ is the wave energy flux at point i with WECs. The same statistical indicators used for wave height were computed for wave energy flux to evaluate the effectiveness of the WEC array in reducing wave energy propagation.

2.4.2. Erosion mitigation

To quantify the long-term morphodynamic impact of the WEC array on coastal erosion, an area-integrated approach was applied using cumulative erosion and sedimentation results extracted from the same control zone used for wave attenuation analysis. Located directly landward of the WaveRoller array, this control zone enabled a consistent spatial comparison between the baseline (no-WEC) and with-WEC scenarios over 1-, 10-, and 20-year morphodynamic simulations. Three key metrics were used to assess erosion mitigation:

2.4.2.1. Total change in sediment volume. The net difference in cumulative sediment volume between the no-WEC and WEC scenarios was computed as:

$$V_{\text{sediment}} = \sum_{i=1}^{N} \left(E_{\text{WEC},i} - E_{\text{noWEC},i}\right) \cdot A_{\text{cell}} \tag{5}$$

where $E_{\text{noWEC},i}$ and $E_{\text{WEC},i}$ are the cumulative erosion or accretion values (in meters) at grid cell i, A_{cell} is the area of a single grid cell, and N is the number of cells in the control zone. A positive value of V_{sediment} indicates a reduction in net erosion or an increase in sediment deposition due to the presence of the WEC array.

2.4.2.2. Percentage Erosion reduction. The effectiveness of the WEC array in reducing erosion was evaluated using the percent reduction in net sediment loss, calculated as:

$$\eta = \frac{V_{\text{sediment}}}{|V_{\text{noWEC}}|} \times 100 \tag{6}$$

where the baseline sediment volume is:

$$V_{\text{noWEC}} = \sum_{i=1}^{N} E_{\text{noWEC},i} \cdot A_{\text{cell}} \tag{7}$$

Taking the absolute value of V_{noWEC} ensures consistency regardless of whether the control zone experienced net erosion (negative) or deposition (positive). A positive η indicates that the WEC array reduced sediment loss or increased deposition; a negative η indicates that erosion was enhanced relative to the baseline.

2.4.2.3. Sediment retention per unit area. To normalize mitigation performance by spatial extent, sediment retention per unit area was calculated as:

$$R = \frac{V_{\text{sediment}}}{A_{\text{zone}}} \tag{8}$$

where the total control zone area is defined as:

$$A_{\text{zone}} = N \cdot A_{\text{cell}} \tag{9}$$

This metric provides a standardized measure of sediment retention or loss per square meter and enables comparison across sites with different spatial footprints.

2.5. Wave farm energy production

To evaluate the energy output potential of the WEC array, several performance metrics were computed using the WEC power matrix (Fig. 4) in combination with the wave climate data extracted from the Delft3D model. The model outputs hourly values of H_{sig} and mean wave period (T_e) across the simulation period, which were used to construct a wave resource characterization matrix. Unlike prior studies that rely on generic offshore wave conditions, this analysis integrates field-validated, nearshore wave model outputs to produce high-resolution, site-specific energy estimates for a WEC array. The evaluation of the energy production and performance followed the procedure of previous studies [6,15,48].

The energy production, E_0, was calculated by combining the WEC power output P_i (in kW) for each sea state with its occurrence, $O_{b,i}$ (in hours) as:

$$E_0 = \sum_{i=1}^{n} P_i \cdot O_{b,i} \tag{10}$$

where n is the total number of sea state bins defined by combinations of H_{sig} and T_e. This yielded the total annual energy production (in MWh) of the WEC array at the selected deployment site. To enable comparison across devices or configurations, the capacity factor, C_f was computed as:

$$C_f = \frac{E_0}{P_r \cdot h} \times 100 \tag{11}$$

where P_r is the rated power of the WEC array and h is the number of hours in a year.

The capture width CW quantifies the effective width of ocean space from which wave energy is captured and is defined as:

$$CW = \frac{P}{J} \tag{12}$$

where P is the power output (kW) from the device and J is the wave power per unit wave crest length (kW/m). The capture width ratio (CWR), which normalizes the captured power by the device's characteristic width, B (12.5 m in this case), was calculated as:

$$CWR = \frac{P}{J \cdot B} \times 100 \tag{13}$$

It is important to clarify that the CWR was not prescribed as a model input. Instead, energy production and CWR were calculated separately using the approach of previous studies (Eq. 13) [12,15,6], based on the modelled wave conditions at the WEC location and the device-specific power matrix.

2.6. Model scenarios

To investigate the trade-offs between coastal protection and renewable energy generation, a total of nine simulation scenarios were designed by varying two key design parameters of the Wave Energy Converter (WEC) array: gap spacing and distance from the shoreline. These parameters are known to significantly influence the hydrodynamic and morphodynamic impacts of wave farms, as well as their energy extraction efficiency.

The WEC array used in the simulations was modelled as a linear array of ten WaveRoller devices, each with a characteristic width of 12.5 m. Gap spacing was defined as a multiple of device width (D), with three values considered: 2D (25 m), 4D (50 m), and 6D (75 m). Similarly, the distance from the shoreline was varied across three positions: 450 m, 600 m, and 750 m.

The combination of gap spacing and distance from shore yielded nine unique WEC configurations, as summarized in Table 2. All other model

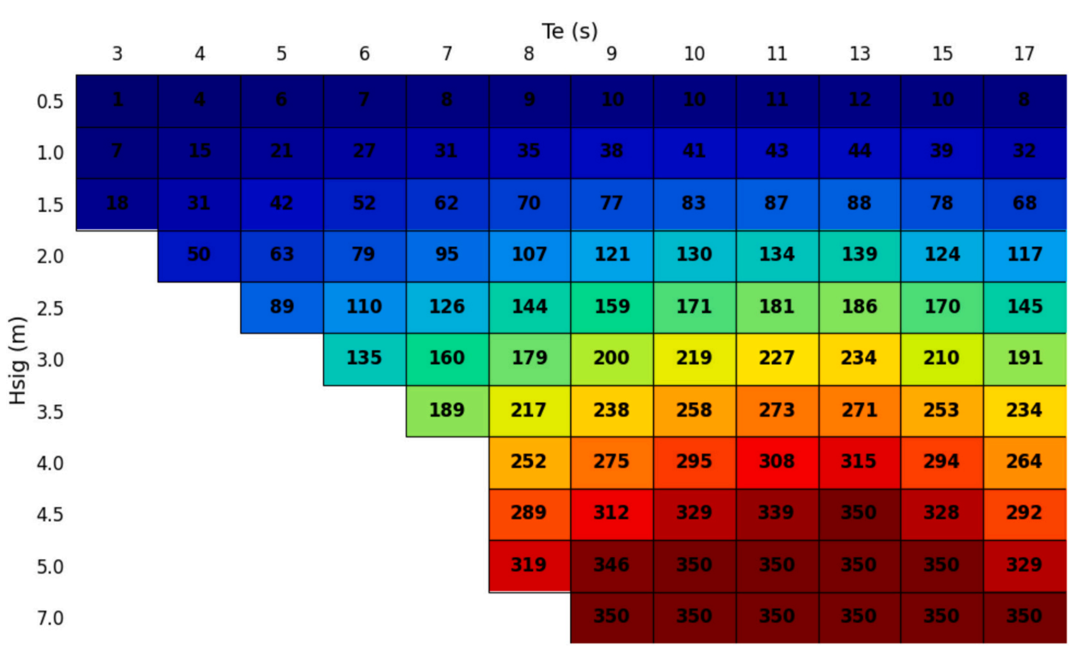

Fig. 4. Power matrix for the WaveRoller device showing mean power output (kW) as a function of H_{sig} and T_e.

Table 2
Wave Energy Converter (WEC) Array Design Configurations used in the Sensitivity Scenarios

Scenario	Gap Spacing	Distance from Shore
S1	2D (25 m)	450 m
S2	2D (25 m)	600 m (baseline)
S3	2D (25 m)	750 m
S4	4D (50 m)	450 m
S5	4D (50 m)	600 m
S6	4D (50 m)	750 m
S7	6D (75 m)	450 m
S8	6D (75 m)	600 m
S9	6D (75 m)	750 m

conditions including wave climate, tidal forcing, and morphological settings were held constant across scenarios to isolate the effects of WEC array geometry. In the sensitivity scenarios, the width of the control zone was adjusted to match the length of each WEC array, which varied with gap spacing. As a result, the spatial area of the control zone differed across scenarios. To ensure comparability, all erosion mitigation metrics were normalized per unit area (m^3/m^2), and spatial attenuation statistics were interpreted in relative terms (e.g., percent of grid points with >10 % attenuation) rather than absolute coverage. Each scenario was simulated over a one-year period (October 2009 to October 2010), with performance evaluated using the wave attenuation and morphodynamic impact metrics (Section 2.3) and the energy production methodology (Section 2.4). The goal was to assess how different layouts affect both sediment retention and energy output, enabling a comparative analysis to identify potential trade-offs or optimal configurations.

3. Results

3.1. Model validation

Calibration was conducted over the period from 29 October 2009 to 9 March 2010, during which model parameters were adjusted to improve agreement between simulated and observed wave and morphodynamic conditions. The final parameter set used in the model included a wave breaking coefficient (γ) of 0.78, the default wind drag coefficient, and a JONSWAP bottom friction coefficient of 0.067 m^2s^{-3}. Sediment transport was computed using the Van Rijn formulation, with wave and current related bedload and suspended load transport factors set to 0.3.

Wave model validation was conducted over the period from 1 June 2010 to 29 October 2010 using the ADCP dataset described in Section 2.2.3. Fig. 5A presents the time series comparison of modelled and

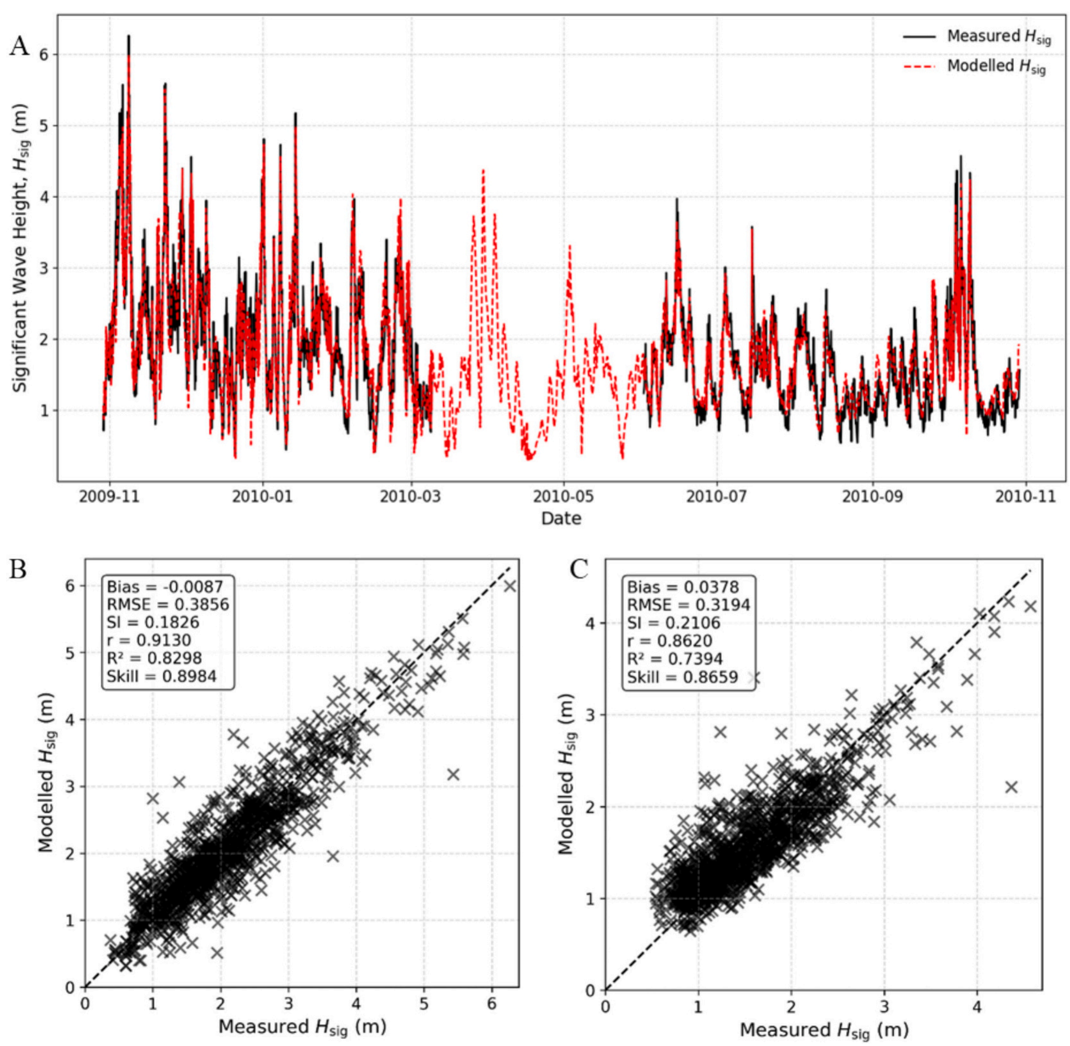

Fig. 5. (A) Time series comparison of measured and modelled significant wave heights (Hsig) over the full simulation period (29 October 2009–29 October 2010) at Almagreira Beach. (B) Scatter plot of measured vs. modelled H_{sig} for the calibration period (29 October 2009–9 March 2010). (C) Scatter plot for the validation period (1 June 2010–29 October 2010). Performance metrics include Bias, RMSE, Scatter Index (SI), Pearson's r, Coefficient of Determination (R^2), and Skill Score. Observational data were obtained from a nearshore ADCP.

measured H_{sig} over the full simulation period, while Fig. 5B and 5C show the corresponding scatter plots for the calibration and validation periods, respectively. The full set of calibration and validation statistics is summarized in Table 3. During the calibration period, the model achieved a bias of −0.0087 m, RMSE of 0.3856 m, scatter index of 0.1826, Pearson's r of 0.9130, $R^2 = 0.8298$, and a skill score of 0.8984. For the validation period, model performance remained high, with a bias of 0.0378 m, RMSE of 0.3194 m, scatter index of 0.2106, Pearson's r of 0.8620, $R^2 = 0.7394$, and a skill score of 0.8659.

These results indicate that the model performed well in replicating wave conditions across both periods. The low bias values suggest that the model does not consistently over- or underpredict significant wave heights. The RMSE values, although moderate in absolute terms, are small relative to typical wave heights at the site (often exceeding 3.0 m). Model performance met widely accepted standards for coastal wave models, which typically consider results acceptable when simulated values are within 10 % of observations [49]. The high R^2 and Pearson's r values confirm that the model accurately captures the temporal variability in wave conditions, including storm events and seasonal transitions. Scatter index values and skill scores reflect consistently high overall model accuracy. These metrics demonstrate the model's capability to simulate wave transformation processes at Almagreira Beach and support its application in evaluating the effects of WaveRoller deployments.

Water level validation was conducted for the month of October 2010 using water level data from the same ADCP. This period was chosen because it captures a full spring–neap tidal cycle, enabling assessment of the model's ability to simulate tidal variability over a representative interval. The validation results are presented in Fig. 6A (time series comparison) and Fig. 6B (scatter plot) and summarized in Table 3.

The model showed excellent performance in reproducing tidal fluctuations, with a bias of 0.006 m, RMSE of 0.119 m, scatter index of 0.178, $R^2 = 0.977$, and a skill score of 0.981. These values indicate that the model accurately simulates both the magnitude and timing of tidal elevations at the site, with minimal error. Given that the tidal range at the site is moderate and the ADCP is located in ~27 m water depth, an RMSE of ~12 cm is well within acceptable limits for coastal process models. Validation was limited to one month to allow clear visualization of spring–neap dynamics and maintain consistency with the wave validation period. This approach aligns with established practice in coastal modelling, where short, representative validation windows are commonly used to assess tidal performance.

Morphodynamic validation was carried out using bathymetric and topographic survey data collected on 28 June 2010, approximately midway through the validation period. A representative cross-shore transect located near the WaveRoller deployment site was used to compare initial, measured, and modelled bed levels (Fig. 7). The model reproduced both the magnitude and trend of bed level change including nearshore erosion. The validation results for the bed level changes, also reported in Table 3, confirm strong agreement between the modelled and measured profiles. Quantitative comparison yielded a bias of 0.010 m, RMSE of 0.334 m, and an R^2 of 0.998, indicating strong agreement. The high R^2 value confirms that the model accurately captures the spatial trend in morphodynamic response, while the RMSE reflects small local deviations in magnitude which are typical in sediment transport simulations due to the natural variability in seabed features.

Table 3
Calibration and validation statistics for wave heights and bed level changes. Bed level validation is based on a cross-shore profile during the validation period.

Metric	Wave Height (Calibration)	Wave Height (Validation)	Water Level (Validation)	Bed Level (Validation)
Bias (m)	−0.0087	0.0378	0.0056	0.010
RMSE (m)	0.3856	0.3194	0.1192	0.334
Scatter Index	0.1826	0.2106	0.178	–
Pearson's r	0.9130	0.8620	0.9885	–
R^2	0.8298	0.7394	0.9770	0.998

Although the first half of the simulation period was used for calibration and the second half for validation, the entire one-year dataset (29 October 2009 to 29 October 2010) was used for the scenario simulations presented in subsequent sections. This was justified on the basis that the selected year represents a typical range of wave and morphodynamic conditions at the site, including both storm and calm periods. Using the full record ensures that seasonal variability is fully captured in the long-term impact assessment.

3.2. *Wave attenuation*

Wave attenuation was assessed by comparing modelled H_{sig} from simulations with and without the WaveRoller array across three representative sea state conditions: storm (23 November 2009 13:00), moderate (9 December 2009 19:00), and low wave energy (30 June 2010, 15:00). Spatial patterns of wave height and direction under baseline and WEC scenarios are shown in Fig. 8 for storm, moderate, and low wave conditions. Across all cases, a clear shadow zone forms in the lee of the WEC array where wave heights are significantly reduced.

Spatial wave height data was extracted from the defined control region located directly behind the WEC array (Fig. 8), and attenuation was calculated point-by-point. The control zone consisted of 451 grid cells, corresponding to an area of approximately 143,437.5 m^2, and remained constant across all wave conditions. The statistical analyses are summarized in Table 4.

The spatial analysis of wave attenuation within the control zone revealed a mean reduction in significant wave height of 13.16 % during storm conditions, 14.17 % during moderate wave conditions, and 16.92 % during low energy conditions (Table 4). The maximum attenuation exceeded 65 % during storm and moderate conditions and approached 59 % during low conditions. The 75th percentile attenuation increased progressively from 22.93 % (storm) to 27.81 % (moderate) and 30.52 % (low), indicating a higher spatial extent of attenuation under lower wave energy conditions. Standard deviation values ranged between 16.5 % and 18.2 %, reflecting substantial spatial variability in wave height reduction across the control area. Notably, the proportion of grid points experiencing greater than 10 % wave attenuation rose from 43.5 % under storm conditions to 64.97 % under low energy conditions, suggesting that the WaveRoller array was relatively more effective in dissipating wave energy under calmer sea states.

The wave energy flux attenuation within the control zone demonstrated mean reductions of 28.81 %, 31.45 %, and 36.39 % under storm, moderate, and low wave energy conditions, respectively (Table 5). Maximum localized reductions reached 87.80 % under storm conditions and exceeded 90 % under moderate conditions. The 75th percentile attenuation values increased steadily from 40.82 % (storm) to 47.62 % (moderate) and 51.25 % (low), indicating enhanced spatial coverage of energy dissipation at lower wave energy levels. The proportion of grid points experiencing greater than 10 % attenuation rose from 81.37 % under storm conditions to 92.02 % under low energy conditions, emphasizing the broader spatial effectiveness of the WaveRoller array in dissipating wave energy flux, particularly under calmer sea states.

These results reveal that the WEC array is more effective at reducing wave energy flux under lower and moderate wave conditions, which comprise a significant portion of the annual wave climate. While storm waves overwhelm the array's ability to attenuate a large share of energy across the entire zone, localized reductions remain significant and may contribute to erosion mitigation in targeted areas.

3.3. *Long term Morphodynamic impacts*

The cumulative erosion and sedimentation results showed that the

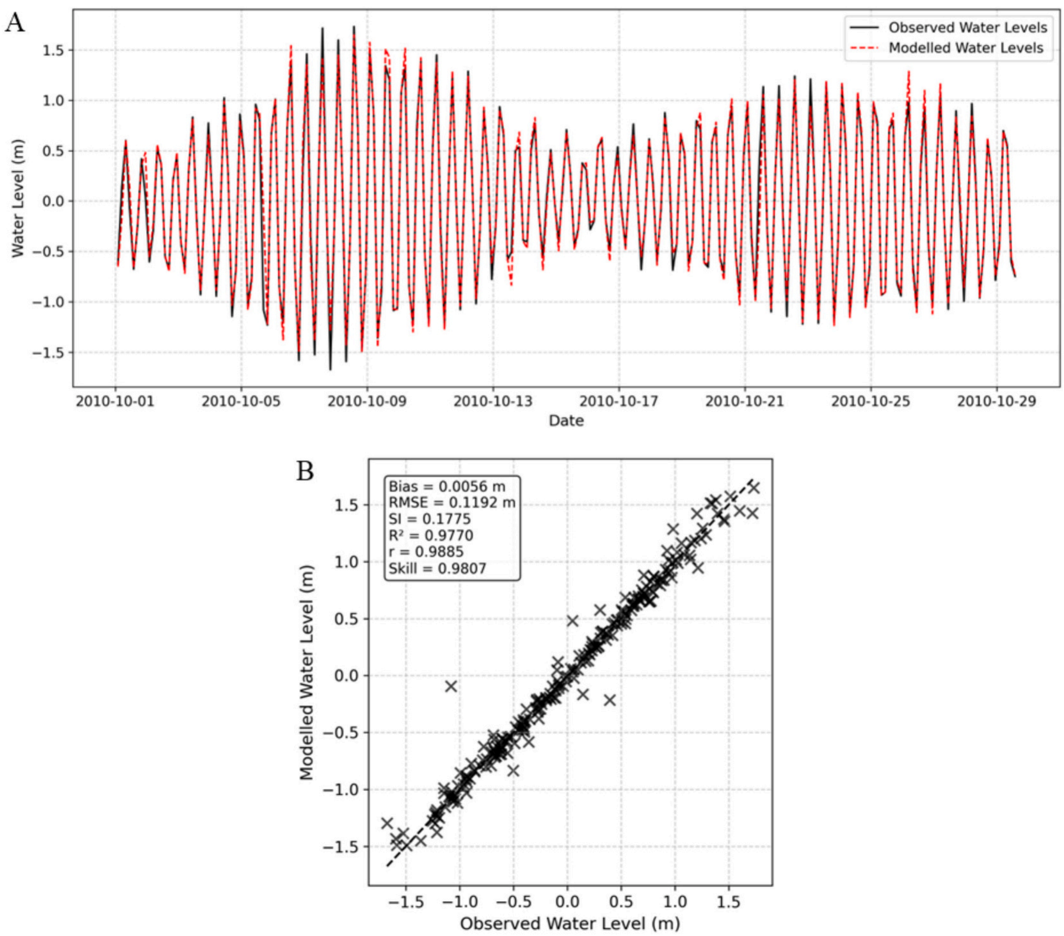

Fig. 6. (A) Time series and (B) scatter plot comparing measured and modelled water levels at Almagreira Beach for October 2010. Metrics include bias, RMSE, SI, R^2, Pearson's r, and skill score. Data from a nearshore ADCP (~27 m depth).

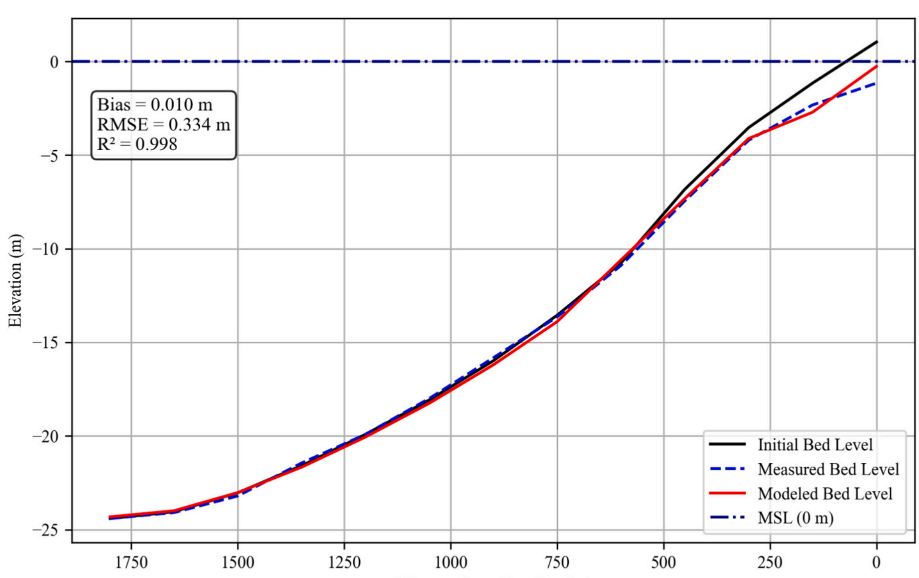

Fig. 7. Validation of modelled bed levels against measured and initial profiles along a cross-shore transect at Almagreira Beach.

presence of the WEC array consistently reduced net sediment loss within the control zone. Fig. 9 presents the spatial distribution of cumulative morphodynamic changes for the baseline (left) and WEC (right) scenarios after 1, 10, and 20 years of simulation. In the absence of WECs, substantial erosion was observed along the nearshore zone for all simulation durations. By contrast, the WEC scenario exhibited a clear reduction in erosion and localized sediment retention immediately shoreward of the array.

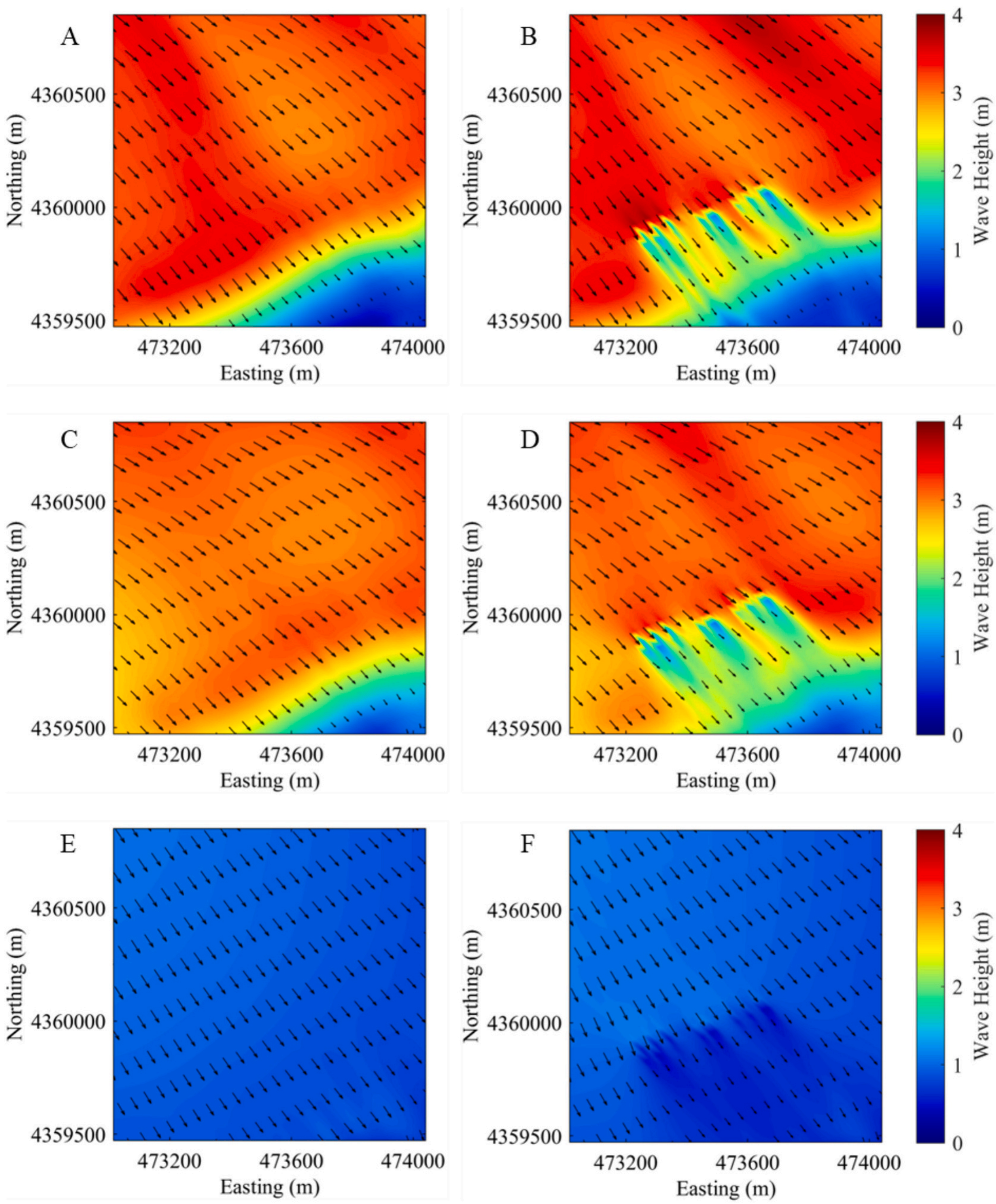

Fig. 8. Spatial distribution of significant wave heights for baseline (left) and WEC (right) scenarios under different sea states. (A–B) Storm condition; (C—D) Moderate condition; (E–F) Low-energy condition. Black arrows indicate wave direction.

Table 4
Wave attenuation statistics within the control zone for storm, moderate, and low wave conditions, based on point-by-point comparison between with-WEC and no-WEC simulations.

Condition	Mean (%)	75th Percentile (%)	Max (%)	Standard Deviation (%)	% > 10 % Attenuation
Storm	13.16	22.93	65.48	16.52	43.5
Moderate	14.17	27.81	65.07	18.22	52.33
Low	16.92	30.52	58.52	17.90	64.97

Table 5
Wave energy flux attenuation statistics for storm, moderate, and low wave conditions, based on point-by-point comparison between with-WEC and no-WEC scenarios.

Condition	Mean (%)	75th Percentile (%)	Max (%)	Standard Deviation (%)	% > 10 % Attenuation
Storm	28.81	40.82	87.80	21.65	81.37
Moderate	31.45	47.62	90.23	22.46	86.25
Low	36.39	51.25	82.56	19.15	92.02

After 1 year (Fig. 9A and B), differences between the two scenarios are minor but detectable, especially in the lee of the WEC array. By 10 years (Fig. 9C and D), more pronounced protection is observed, with the no-WEC scenario showing deeper and more widespread erosion. At 20 years (Fig. 9E and F), the WEC-protected scenario maintains significantly less erosion and deposition onshore.

Quantitative results for the 1-, 10-, and 20-year simulations are summarized in Table 6. In the 1-year simulation, The WEC array reduced

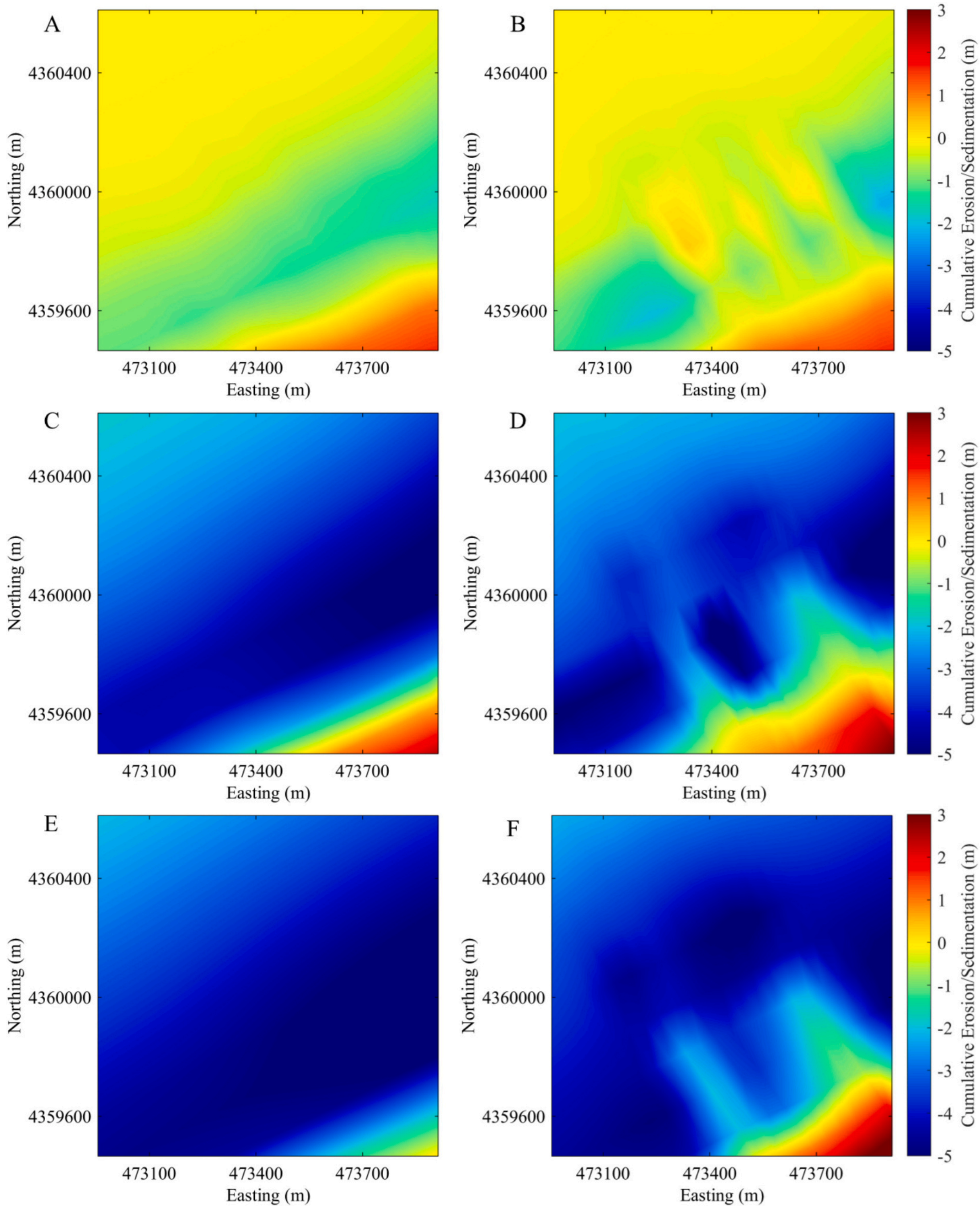

Fig. 9. Cumulative erosion and sedimentation without WECs and with WECs over 1 year (A–B), 10 years (C—D), and 20 years (E–F)

Table 6
Summary of erosion mitigation metrics within the control zone for the 1-, 10-, and 20-year simulations, including cumulative sediment volume retained, incremental volume retained, percentage erosion reduction, and retention per unit area.

Simulation Period	Cumulative Volume Retained (m^3)	Incremental Volume Retained (m^3)	Percent Erosion Reduction (%)	Retention per Unit Area (m^3/m^2)
1 Year	47,731	47,731	41.15	0.333
10 Years	252,073	204,342	50.44	1.757
20 Years	278,427	26,354	41.93	1.941

net sediment loss by approximately 47,731 m^3 compared to the baseline scenario, corresponding to a 41.15 % reduction in erosion relative to the baseline. The retention per unit area was 0.333 m^3/m^2, indicating a strong localized mitigation effect during the early stage of deployment.

Over the 10-year period, the total volume of sediment retained increased substantially to 252,073 m^3, with the percent reduction in erosion rising to 50.44 %. The retention per unit area also increased to 1.757 m^3/m^2, suggesting that the WECs enhanced sediment trapping effectiveness over the first decade. The incremental volume retained between 1 and 10 years was 204,342 m^3, indicating that the majority of the sediment retention occurred during this period.

By 20 years, the cumulative retained volume further increased to 278,427 m^3, with a 41.93 % reduction in erosion and a retention per unit area of 1.941 m^3/m^2. However, the incremental sediment retention between 10 and 20 years was only 26,354 m^3, a substantial decrease compared to the gain in the first decade.

3.4. Energy production

The annual energy output of the WaveRoller array was estimated by coupling the modelled wave conditions at Almagreira Beach with the WEC's power matrix (Fig. 4). A wave resource matrix was generated from the Delft3D model outputs, which provided hourly values of H_{sig} and T_e over a full year. These values were discretized into sea state bins and combined with the power matrix to compute the energy extracted by the WECs under each condition.

Fig. 10 presents the wave resource matrix, showing the distribution of sea state occurrence (in hours/year) and the corresponding wave energy (in MWh/m/year). The most frequent conditions occurred within H_{sig} bins of 1.0–2.5 m and T_e bins of 6–11 s, with an estimated peak energy density reaching over 7 MWh/m/year. Superimposed isolines indicate deep-water wave power flux levels of 25, 100, and 250 kW/m.

Table 7 summarizes the key performance metrics of the system. The device operated at an average capacity factor of 18.34 %, a value consistent with nearshore oscillating wave surge converters, demonstrating efficient conversion despite seasonal variability, with 1606.6 full load hours. The theoretical wave energy incident on the device was 1126.5 MWh, based on an annual wave energy flux of 93.88 MWh/m. The average width was 6.36 m reinforcing the system's ability to efficiently utilize the site's wave climate.

Fig. 11 shows the modelled instantaneous power output from a single WaveRoller device over the one-year simulation. Clear seasonal trends are evident, with higher power generation during the winter months and reduced performance during summer. These fluctuations highlight the variability of the wave climate at the site, underlining the importance of seasonal planning for grid integration or hybridization.

Cumulative energy production is illustrated in Fig. 12. The green line indicates the cumulative energy output of the WEC, while the dashed red line represents the total theoretical wave energy available to a 12 m wide device. The close alignment between the two curves in the early stages gives way to a consistent divergence, with the WEC capturing approximately 49.9 % of the available energy by the end of the year. This corresponds to a total annual energy output of 562.3 MWh for a single device and 5623 MWh when scaled to an array of 10 devices.

Table 7
Summary of energy production and performance metrics based on the modelled deployment of 10 WaveRoller devices at Almagreira Beach over a one-year period.

Metric	Value	Unit
Annual Energy Production (1 WEC)	562.3	MWh/year
Annual Energy Production (10 WECs)	5623.0	MWh/year
Rated Power (per device)	350	kW
Capacity Factor	18.34	%
Full Load Hours	1606.6	hours/year
Theoretical Wave Energy per meter	93.88	MWh/m/
Theoretical Wave Energy (12 m WEC width)	1126.5	MWh/year
Average Capture Width	6.36	m
Capture Efficiency	49.9	%

3.5. Sensitivity to design parameters

The results of the nine sensitivity scenarios conducted to evaluate the impact of WaveRoller array design on coastal protection and energy production are summarized in Table 8 which shows how changes in these parameters influence wave attenuation, erosion mitigation, and energy output.

Wave attenuation was most effective at tighter spacing and greater offshore distance. Scenario S3 (2D spacing, 750 m offshore) achieved the highest mean wave attenuation (26.73 %) and the highest 75th percentile (32.67 %), indicating strong performance even under higher-energy wave conditions. Conversely, increasing the spacing to 6D

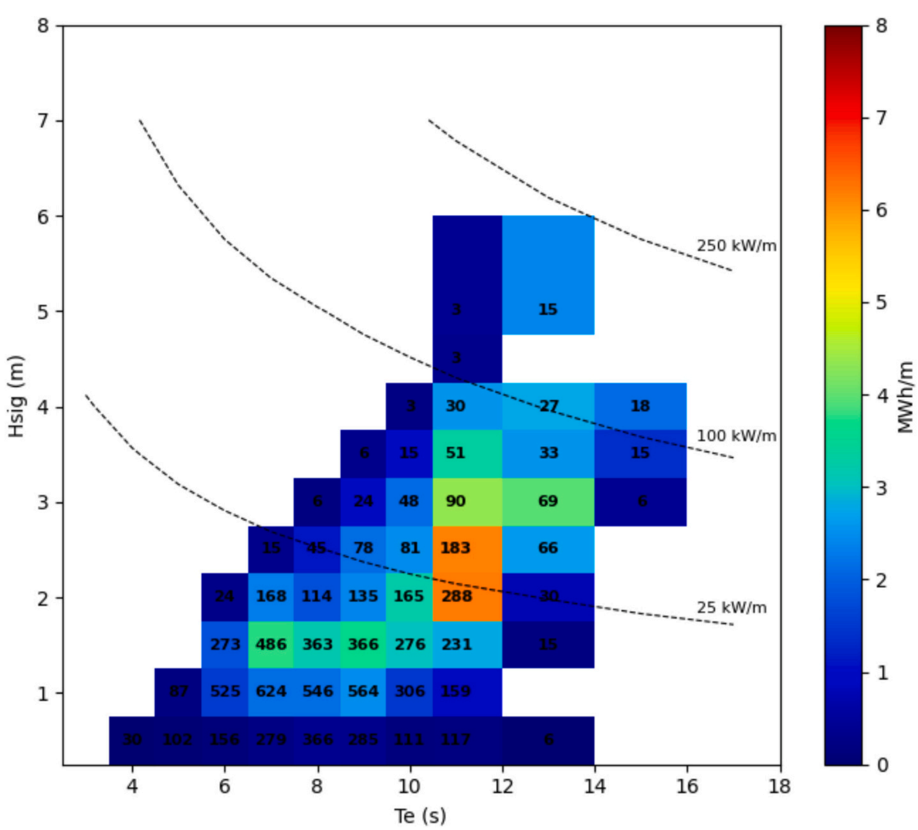

Fig. 10. Wave resource matrix showing the annual wave energy distribution as a function of Hsig and Te

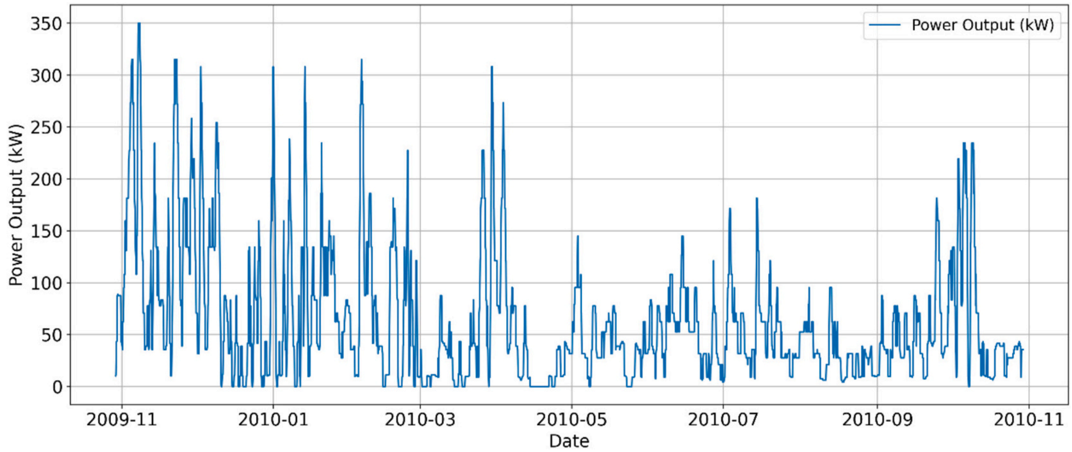

Fig. 11. Time series of simulated power output (kW) from the wave energy converter over a one-year period (October 2009–October 2010), based on mapped sea states and the device power matrix.

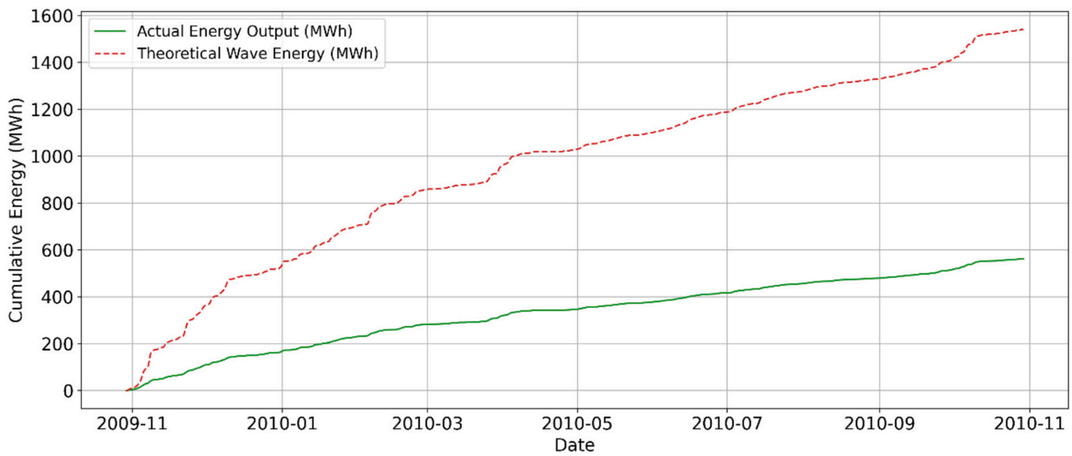

Fig. 12. Cumulative energy production. The green line indicates the cumulative energy output of the WEC, while the dashed red line represents the total theoretical wave energy available to a 12 m wide device. (For interpretation of the references to colour in this figure legend, the reader is referred to the web version of this article.)

Table 8
Summary of sensitivity analysis results for nine WaveRoller array configurations. Scenarios vary by gap spacing (2D, 4D, 6D) and offshore distance (450 m, 600 m, 750 m)

Scenario	Spacing	Distance (m)	Energy Production (MWh)	Mean Wave Attenuation (%)	75th Percentile Attenuation (%)	Sediment Retention (m^3)	Retention per unit area (m^3/m^2)
S1	2D	450	2286.8	6.33	8.36	26,796.8	0.19
S2	2D	600	5623	14.17	18.56	47,731	0.33
S3	2D	750	5845.9	26.73	32.67	43,933.8	0.32
S4	4D	450	2286.8	4.23	6	19,644.8	0.15
S5	4D	600	5623	4.19	5.83	15,950.6	0.11
S6	4D	750	5845.9	5.24	7.34	8334.8	0.06
S7	6D	450	2286.8	2.03	2.68	16,882.1	0.07
S8	6D	600	5623	3.86	5.3	12,072.1	0.04
S9	6D	750	5845.9	7.01	9.93	26,483.7	0.09

significantly reduced attenuation across all distances, with S7 (6D, 450 m) showing a mean reduction of only 2.03 %.

Erosion mitigation followed a similar trend. S2 (2D, 600 m) retained the largest sediment volume (47,731 m^3) and had the highest normalized sediment retention per unit area (0.333 m^3/m^2). Although S3 produced slightly less sediment retention overall (43,933.8 m^3), it achieved comparable normalized performance (0.319 m^3/m^2) due to its slightly smaller control area. In contrast, S6 (4D, 750 m) and S8 (6D, 600 m) had the lowest retention values, both in total and per unit area.

Energy production increased with distance from shore, as expected due to greater wave exposure. The transition from 450 m to 750 m yielded ~25 % higher energy production on average, regardless of spacing. However, spacing had negligible influence on energy output since the same number of devices were simulated. The increase in energy from S2 to S3 (5623.0 to 5845.9 MWh) highlights the potential energy gain from placing arrays farther offshore although this came with a trade-off in reduced sediment retention.

These results highlight a clear trade-off between energy maximization and coastal protection. Scenarios with 2D spacing consistently outperformed wider spacings in both wave attenuation and erosion mitigation. Among all scenarios, S2 (2D, 600 m) appears to offer the best compromise achieving strong energy output, highest sediment retention per area, and balanced wave attenuation. S3 (2D, 750 m) offers the highest wave attenuation and energy, but with a moderate decline in erosion mitigation.

To better understand the trade-offs between these competing objectives, three Pareto plots were constructed (Fig. 13). Fig. 13A compares energy production against normalized sediment retention per unit area. Scenarios located on the upper-right portion of the plot (notably S2 and S3) are Pareto-optimal, meaning they offer the best combined performance. Fig. 13 B compares energy production with mean wave attenuation, again highlighting S3 as the strongest performer in terms of wave attenuation and energy production. The 3D Pareto plot (Fig. 13C) integrates all three objectives: energy, attenuation, and sediment retention and clearly illustrates that no single scenario dominates in all three categories. Instead, S2 and S3 emerge as optimal configurations depending on whether the priority is erosion mitigation or wave attenuation.

These results highlight a clear trade-off between energy maximization and coastal protection. Scenarios with 2D spacing consistently outperformed wider spacings in both wave attenuation and erosion mitigation. Among all scenarios, S2 (2D, 600 m) appears to offer the best compromise — achieving strong energy output, highest sediment retention per area, and balanced wave attenuation. S3 (2D, 750 m) offers the highest wave attenuation and energy, but with a moderate decline in erosion mitigation.

Overall, the results reinforce the importance of WEC array configuration in optimizing the dual objectives of renewable energy production and coastal protection. Designs with moderate spacing and intermediate offshore distance deliver the most balanced performance. This represents one of the first studies to quantitatively evaluate the trade-offs between energy generation and coastal protection in wave farm design using a multi-objective framework.

4. Discussion

4.1. Long term impacts of wave farms on Morphodynamics and coastal protection

The long-term morphodynamic simulations carried out in this study represent one of the first efforts to assess the cumulative coastal protection benefits of a wave farm over multi-year to decadal timeframes. Using a coupled 2DH hydrodynamic, spectral wave and sediment transport model, bed level changes over a 20-year equivalent period were simulated. This allowed for the evaluation of impacts of wave farms on coastal protection through wave attenuation and erosion mitigation beyond the storm term periods typically used in previous studies [1–4,9,34,37].

The cumulative results revealed a consistent reduction in net sediment loss across all timeframes due to the presence of the WEC array. After one year, the WECs retained approximately 47,731 m^3 of sediment within the control zone, corresponding to a 41.15 % reduction in erosion

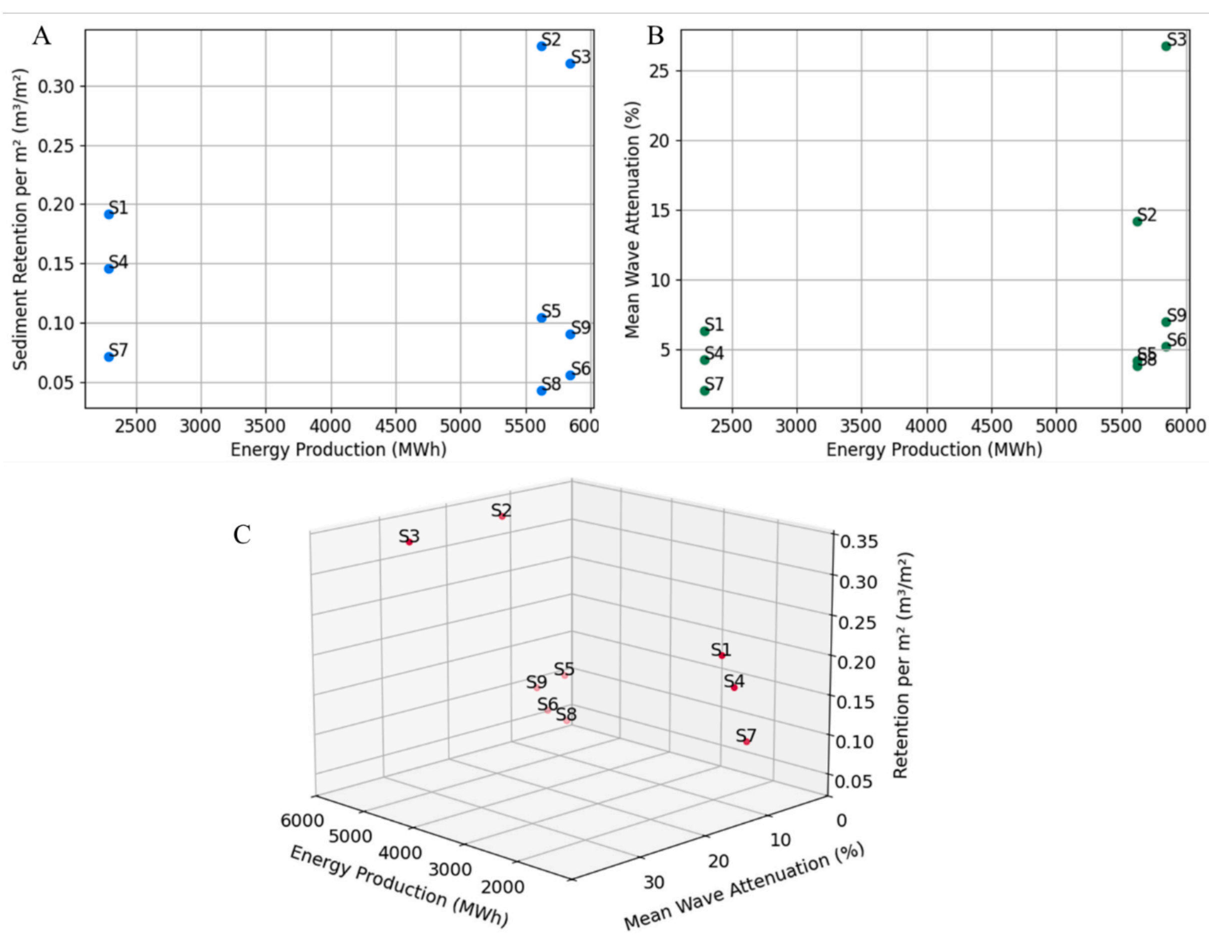

Fig. 13. Multi-objective Pareto analysis of WaveRoller array configurations. (A) Trade-off between energy production and sediment retention per unit area. (B) Trade-off between energy production and mean wave attenuation. (C) 3D Pareto plot integrating energy production, mean wave attenuation, and sediment retention per unit area.

relative to the baseline. This increased substantially after ten years to 252,073 m^3 (50.44 % reduction), but over the subsequent decade, only an additional 26,354 m^3 was retained, bringing the 20-year total to 278,427 m^3 (41.93 % reduction). The reduced marginal gain in the final decade suggests that the sediment system may have approached a dynamic equilibrium, wherein the rate of erosion and deposition stabilizes due to long-term adjustments in bed morphology and wave energy dissipation. It should also be noted that the percentage reduction in erosion was similar to the results obtained from previous studies [9,42] in which percentage erosion mitigation ranged from 15 to 45 % (Boodoo, Wakeyama, and Cross 2025)

A key methodological contribution of this study is the normalization of sediment retention per unit area, which allows for direct comparison between deployment configurations independent of model domain size. This metric enables a spatially explicit understanding of WEC performance and may prove valuable for future studies comparing erosion mitigation potential across different coastal settings or device layouts.

The results also suggest that WEC arrays can provide rapid initial erosion mitigation, with the majority of cumulative sediment retention occurring in the first decade. This early benefit is particularly relevant for highly erodible or sediment-deficient coasts, where initial seabed stabilization is critical to long-term shoreline resilience.

Another novel outcome of this study is the evaluation of wave attenuation under varying sea state conditions over the course of a full year. The results showed that attenuation was most spatially extensive under low wave energy conditions. While storm conditions produce higher localized attenuation, the broader spatial effectiveness of the array in moderate and low conditions suggests that WECs may offer continuous, low-intensity protection that accumulates over time. This finding supports the use of WECs as hybrid protection systems, not solely reliant on peak performance during extreme events, but capable of delivering consistent suppression of erosive energy under everyday conditions.

From a practical standpoint, this erosion mitigation benefits also carry monetary value. If we conservatively estimate nourishment costs between €10 and €20 per m^3 of sediment which is typical for beach nourishment operations in Europe [25], the 278,427 m^3 retained over 20 years represents a potential cost savings of €2.8 to €5.6 million. This reframes the morphodynamic role of WECs as not just a secondary benefit but a directly quantifiable asset within a broader coastal management and energy planning framework. While further refinement is needed to fully integrate these values into techno-economic models, this approach presents a new pathway for recognizing and accounting for the multi-functional benefits of wave farms.

4.2. Energy production

The simulated annual energy production for a single WaveRoller device was 562.3 MWh, or 5623 MWh for the modelled array of ten devices, corresponding to a capacity factor of 18.34 %. This aligns well with performance reported in previous studies of oscillating wave surge converters [6,12] and confirms the suitability of Almagreira Beach for wave energy generation.

The energy production results indicate effective energy extraction across a wide range of sea states, particularly given the nearshore location. Energy output closely tracked the site's seasonal wave regime. Winter months (December to February) produced the highest energy, with an average monthly output of ∼67 MWh per device. In contrast, summer months (June to August) yielded an average of ∼28 MWh per device which was less than half the winter output. These results demonstrate that WaveRoller arrays can achieve high performance in suitable nearshore environments, and that device-site matching is critical for maximizing both efficiency and seasonal reliability.

4.3. Dual objective design considerations

To explore how wave farm layout influences both energy generation and coastal protection, nine scenarios were simulated by systematically varying gap spacing (2D, 4D, 6D) and distance from shore (450 m, 600 m, 750 m). The results demonstrate clear trade-offs between performance objectives: while greater offshore distances improve energy capture due to higher wave exposure, tighter spacing enhances wave attenuation and erosion mitigation. These findings highlight the complex interplay between hydrodynamic forces and array design and underscore the need for multi-objective optimization when designing wave farms for dual use.

Scenarios with 2D spacing consistently outperformed wider layouts in terms of both wave attenuation and sediment retention. Among these, Scenario S2 (2D spacing, 600 m offshore) achieved the best overall balance: it delivered 5623 MWh/year, retained the most sediment (47,731 m^3), and exhibited strong wave attenuation (mean: 14.17 %, 75th percentile: 18.56 %). Scenario S3 (2D, 750 m), on the other hand, maximized energy production (5846 MWh/year) and achieved the highest mean wave attenuation (26.73 %) but this came at a slight cost in sediment retention due to its smaller nearshore influence zone.

To visualize these trade-offs, a set of two-dimensional and three-dimensional Pareto plots were generated (Fig. 13). These plots illustrate how no single configuration dominates across all objectives, and instead, optimal designs depend on the relative weight assigned to each goal. Scenarios S2 and S3 occupy the Pareto front, offering the best combinations of energy production, erosion mitigation, and wave attenuation with the choice between them dependent on whether protection or energy is prioritized.

In contrast, scenarios with 4D and 6D spacing (S4–S9) consistently showed lower performance across most objectives. For example, S8 (6D spacing, 600 m) and S6 (4D, 750 m) yielded low sediment retention and limited attenuation, despite having similar energy output to their 2D counterparts. This indicates that wider spacing significantly reduces coastal protection benefits without a meaningful gain in energy, and that both spacing and distance interact nonlinearly to influence outcomes.

The broader implication is that wave energy converter arrays should not be treated as static infrastructure optimized for a single outcome. Instead, their placement and spacing can and should be strategically tuned to meet site-specific coastal management and energy objectives. For example, in regions with high erosion risk, tighter spacing and moderate distances may provide co-benefits that justify slightly lower energy output. Conversely, energy-dominant sites can prioritize wider spacing or greater depth placements, provided coastal impacts are acceptable or mitigated.

This framework supports a more flexible and adaptive approach to wave farm planning, grounded in evidence-based modelling and spatially explicit performance metrics. It also strengthens the case for regulatory frameworks that evaluate marine energy infrastructure not only on energy yield, but on broader environmental and coastal system outcomes.

4.4. Implications and future research directions

This study presents one of the first long-term, process-based investigations into the dual role of wave farms for renewable energy production and coastal protection. While previous research has largely focused on short-term simulations or isolated performance metrics, this work combines decadal scale morphodynamic modelling, detailed wave energy output calculations, and multi-objective trade-off analysis to assess the co-benefits of WEC deployment. The integration of erosion mitigation, wave attenuation, and energy production into a unified evaluation framework represents a major step forward in the holistic assessment of wave energy projects.

A key aspect of this research lies in the quantification of sediment retention over multi-year timescales, expressed both in volumetric terms and normalized per unit area. This allows the morphodynamic benefits of WECs to be translated into economic terms, for example, by estimating the equivalent cost of avoided beach nourishment. Such estimates can be incorporated into techno-economic models to reduce the perceived levelized cost of electricity (LCoE), thereby improving the competitiveness of wave energy in integrated coastal and energy planning frameworks.

This opens up an important future research direction: the development of hybrid economic valuation models that account for both energy and protection functions of wave farms. By incorporating retained sediment volumes and associated cost savings into project appraisal, decision-makers can better evaluate the full value of wave farms, especially in erosion-prone regions where the economic case for intervention is strong.

In addition, future research should examine the ecological and environmental impacts of wave farms, particularly in nearshore environments where benthic habitats, sediment-dwelling organisms, and coastal ecosystems may be affected. While WECs present a lower-impact alternative to hard coastal defences, their long-term influence on habitat structure, sediment grain size distribution, and local biodiversity remains poorly understood.

While the current study provides valuable insights into how spacing and distance influence performance, the sensitivity analysis was limited to a small number of discrete scenarios. As such, there is a critical need for multi-objective optimization frameworks that identify optimal trade-offs between energy production and coastal protection. Future research should apply formal optimization algorithms such as genetic algorithms or machine learning techniques to better capture complex interactions and site-specific constraints in wave farm design.

5. Conclusion

This study assessed the long-term impacts of a nearshore WaveRoller WEC wave farm on both energy production and coastal morphodynamics. Using a coupled 2DH hydrodynamic, spectral wave and sediment transport model, energy output, wave attenuation, and erosion mitigation over a 20-year equivalent period were evaluated.

The results confirm the potential of wave farms to contribute to both renewable energy and coastal protection. Annual energy production reached 562.3 MWh per device, with a capacity factor of 18.34 % and a capture efficiency of 49.9 %, demonstrating strong performance in a nearshore setting well-matched to the device's power characteristics. The wave farm retained over 278,000 m^3 of sediment across two decades, with a peak normalized retention of 1.941 m^3/m^2. These erosion mitigation benefits, most significant during the early years of operation, translate to an estimated cost savings of €2.8–€5.6 million in avoided nourishment expenditures, highlighting the economic value of incorporating morphodynamic benefits into techno-economic models of wave energy. Wave attenuation was observed across all sea state conditions, with the greatest spatial impact occurring during calm-to-moderate periods, suggesting that wave farms can offer consistent erosion control beyond period of storm activity.

The study also revealed important design trade-offs between energy production and coastal protection, with tighter spacing and moderate offshore distances maximizing sediment retention and wave attenuation, while greater distances improved energy output. A multi-scenario sensitivity analysis and 3D Pareto plots identified optimal configurations, particularly Scenarios S2 (2D spacing, 600 m offshore) and S3 (2D spacing, 750 m offshore), that achieve a balanced performance across both objectives. These findings underscore the need for site-specific, multi-objective optimization in wave farm planning and support a more flexible, benefit-driven approach to WEC deployment.

By quantifying long-term morphodynamic impacts, this research paves the way for framing erosion mitigation in economic terms, applying multi-objective analysis to wave farm design and evaluating dual-use wave farms. Future work should focus on multi-objective optimization strategies, techno-economic integration, and the ecological implications of wave farms.

CRediT authorship contribution statement

Avinash Boodoo: Writing – review & editing, Writing – original draft, Visualization, Validation, Methodology, Investigation, Formal analysis, Conceptualization. **Jeffrey S. Cross:** Writing – review & editing, Supervision, Investigation, Formal analysis. **Christopher Ridgewell:** Writing – review & editing, Resources, Project administration, Investigation, Data curation. **Ville Kortelainen:** Writing – review & editing, Resources, Project administration, Investigation, Formal analysis, Data curation. **Matti Vuorinen:** Writing – review & editing, Resources, Investigation, Formal analysis, Data curation. **Amina Harouna-Mayer:** Writing – review & editing, Resources, Investigation, Data curation.

Declaration of competing interest

The authors declare that they have no known competing financial interests or personal relationships that could have appeared to influence the work reported in this paper. Co-authors from AW-Energy contributed to this study by providing access to site-specific data and technical guidance related to the WaveRoller device.

Acknowledgements

The first author would like to acknowledge the Japan Ministry of Education, Culture, Sports, Science and Technology (MEXT) for financial support through the MEXT Scholarship for graduate studies. The data and support from AW-Energy is greatly appreciated.

Data availability

The data used in this study were provided by AW-Energy and are not publicly available. Requests for access should be directed to AW-Energy and are subject to their approval.

References

[1] Abanades J, Flor-Blanco G, Flor G, Iglesias G. Dual wave farms for energy production and coastal protection. Ocean Coast Manag 2018;160:18–29. https://doi.org/10.1016/j.ocecoaman.2018.03.038.

[2] Abanades J, Greaves D, Iglesias G. Coastal defence through wave farms. Coast Eng 2014;91:299–307. https://doi.org/10.1016/j.coastaleng.2014.06.009.

[3] Abanades J, Greaves D, Iglesias G. Wave farm impact on the beach profile: a case study. Coast Eng 2014;86:36–44. https://doi.org/10.1016/j.coastaleng.2014.01.008.

[4] Abanades J, Greaves D, Iglesias G. Coastal defence using wave farms: the role of farm-to-coast distance. Renew Energy 2015;75:572–82. https://doi.org/10.1016/j.renene.2014.10.048.

[5] Ahn Seongho, Haas Kevin A, Neary Vincent S. Wave energy resource characterization and assessment for coastal waters of the United States. Appl Energy 2020;267:114922. https://doi.org/10.1016/j.apenergy.2020.114922.

[6] Arean N, Carballo R, Iglesias G. An integrated approach for the installation of a wave farm. Energy 2017;138:910–9. https://doi.org/10.1016/j.energy.2017.07.114.

[7] Arguilé-Pérez B, Ribeiro AS, Costoya X, deCastro M, Gómez-Gesteira M. Suitability of wave energy converters in northwestern Spain under the near future winter wave climate. Energy 2023;278:127957. https://doi.org/10.1016/j.energy.2023.127957.

[8] Astariz S, Iglesias G. The economics of wave energy: a review. Renew Sust Energ Rev 2015;45:397–408. https://doi.org/10.1016/j.rser.2015.01.061.

[9] Bergillos Rafael J, López-Ruiz Alejandro, Medina-López Encarnación, Moñino Antonio, Ortega-Sánchez Miguel. The role of wave energy converter farms on coastal protection in eroding deltas, Guadalfeo, southern Spain. J Clean Prod 2018;171:356–67. https://doi.org/10.1016/j.jclepro.2017.10.018.

[10] Bergillos Rafael J, Rodriguez-Delgado Cristobal, Iglesias Gregorio. Wave farm impacts on coastal flooding under sea-level rise: a case study in southern Spain. Sci Total Environ 2019;653:1522–31. https://doi.org/10.1016/j.scitotenv.2018.10.422.

[11] Berrio Y, Rivillas-Ospina G, Ruiz-Martínez G, Arango-Manrique A, Ricaurte C, Mendoza E, et al. Energy conversion and beach protection: numerical assessment of

a dual-purpose WEC farm. Renew Energy 2023;219:119555. https://doi.org/10.1016/j.renene.2023.119555.

[12] Bertram DV, Tarighaleslami AH, Walmsley MRW, Atkins MJ, Glasgow GDE. A systematic approach for selecting suitable wave energy converters for potential wave energy farm sites. Renew Sust Energ Rev 2020;132:110011. https://doi.org/10.1016/j.rser.2020.110011.

[13] Boodoo Avinash, Villarroel-Lamb Deborah. Numerical modelling of the impact of coral reef degradation and sea level rise on coastal protection at the Buccoo reef, Tobago: implications for reef restoration and management strategies. Front Mar Sci 2025;12. https://doi.org/10.3389/fmars.2025.1525438.

[14] Boodoo Avinash, Wakeyama Tatsuya, Cross Jeffrey S. Wave farms for coastal protection: a systematic review of effectiveness, methodologies, and future directions. Ocean Coast Manag 2025;269:107807. https://doi.org/10.1016/j.ocecoaman.2025.107807.

[15] Carballo R, Arean N, Álvarez M, López I, Castro A, López M, et al. Wave farm planning through high-resolution resource and performance characterization. Renew Energy 2019;135:1097–107. https://doi.org/10.1016/j.renene.2018.12.081.

[16] Cheng Yong, Xi Chen, Dai Saishuai, Ji Chunyan, Cocard Margot. Wave energy extraction for an array of dual-oscillating wave surge converter with different layouts. Appl Energy 2021;292:116899. https://doi.org/10.1016/j.apenergy.2021.116899.

[17] Clemente D, Ramos V, Teixeira-Duarte F, Taveira-Pinto FVC, Rosa-Santos P, Taveira-Pinto F. Assessment of electricity production and coastal protection of a nearshore 500 MW wave farm in the north-western Portuguese coast. Appl Energy 2025;379:124950. https://doi.org/10.1016/j.apenergy.2024.124950.

[18] Contestabile Pasquale, Iuppa Claudio, Di Lauro Enrico, Cavallaro Luca, Andersen Thomas Lykke, Vicinanza Diego. Wave loadings acting on innovative rubble mound breakwater for overtopping wave energy conversion. Coast Eng 2017;122:60–74. https://doi.org/10.1016/j.coastaleng.2017.02.001.

[19] Drew B, Plummer AR, Sahinkaya MN. A review of wave energy converter technology. Proc Inst Mech Eng Part A: J Power Energy 2009;223(8):887–902. https://doi.org/10.1243/09576509jpe782.

[20] Fanti V, Jacob J, Pacheco A, Fortes CJEM, Didier E. Effects of varying the transmission coefficient in SNL-SWAN for a wave farm in Peniche. In: Developments in renewable energies offshore. CRC Press; 2020. p. 11–8.

[21] Foteinis S, Tsoutsos T. Strategies to improve sustainability and offset the initial high capital expenditure of wave energy converters (WECs). Renew Sust Energ Rev 2017;70:775–85. https://doi.org/10.1016/j.rser.2016.11.258.

[22] Goda, Y. 1969. "Reanalysis of laboratory data on wave transmission over breakwaters." Report of the Port and Harbour Research Institute 8 (3): 3–18.

[23] Gunn Kester, Stock-Williams Clym. Quantifying the global wave power resource. Renew Energy 2012;44:296–304. https://doi.org/10.1016/j.renene.2012.01.101.

[24] Guo Bingyong, Ringwood John V. A review of wave energy technology from a research and commercial perspective. IET Renew Power Gener 2021;15(14):3065–90. https://doi.org/10.1049/rpg2.12302.

[25] Hudson, Thomas, Kevin Keating, and Angus Pettit. 2015. "Cost estimation for coastal protection–summary of evidence." Environment Agency UK*, Report no. SC080039* 7.

[26] Iglesias G, Carballo R. Wave farm impact: the role of farm-to-coast distance. Renew Energy 2014;69:375–85. https://doi.org/10.1016/j.renene.2014.03.059.

[27] Instituto Hidrográfico. 2011-04-08 2011. SURGE Project – *Technical report on environmental monitoring (IH.45).* Instituto Hidrográfico (Lisbon, Portugal).

[28] Jin Siya, Greaves Deborah. Wave energy in the UK: status review and future perspectives. Renew Sust Energ Rev 2021;143:110932. https://doi.org/10.1016/j.rser.2021.110932.

[29] Lesser GR, Roelvink JA, van Kester JATM, Stelling GS. Development and validation of a three-dimensional morphological model. Coast Eng 2004;51(8):883–915. https://doi.org/10.1016/j.coastaleng.2004.07.014.

[30] Re Lo, Carlo Giorgio Manno, Basile Mirko, Ciraolo Giuseppe. The opportunity of using wave energy converters in a Mediterranean hot spot. Renew Energy 2022;196:1095–114. https://doi.org/10.1016/j.renene.2022.07.010.

[31] López Iraide, Andreu Jon, Ceballos Salvador, Martínez Iñigo, de Alegría, and Iñigo Kortabarria.. Review of wave energy technologies and the necessary power-equipment. Renew Sust Energ Rev 2013;27:413–34. https://doi.org/10.1016/j.rser.2013.07.009.

[32] Losada Miguel A, Giménez-Curto Luis A. Flow characteristics on rough, permeable slopes under wave action. Coast Eng 1980;4:187–206.

[33] Manasseh Richard, Sannasiraj SA, McInnes Kathleen L, Sundar V, Jalihal Purnima. Integration of wave energy and other marine renewable energy sources with the needs of coastal societies. Int J Ocean Climate Syst 2017;8(1):19–36. https://doi.org/10.1177/1759313116683962.

[34] Mendoza Edgar, Silva Rodolfo, Zanuttigh Barbara, Angelelli Elisa, Andersen Thomas Lykke, Martinelli Luca, et al. Beach response to wave energy converter farms acting as coastal defence. Coast Eng 2014;87:97–111. https://doi.org/10.1016/j.coastaleng.2013.10.018.

[35] Mustapa MA, Yaakob OB, Ahmed Yasser M, Chang-Kyu Rheem KK, Koh, and Faizul Amri Adnan.. Wave energy device and breakwater integration: a review. Renew Sust Energ Rev 2017;77:43–58. https://doi.org/10.1016/j.rser.2017.03.110.

[36] Onea Florin, Rusu Liliana, Carp Gabriel Bogdan, Rusu Eugen. Wave farms impact on the coastal processes—a case study area in the Portuguese nearshore. J Mar Sci Eng 2021;9(3):262. https://www.mdpi.com/2077-1312/9/3/262.

[37] Ozkan Cigdem, Mayo Talea, Passeri Davina L. The potential of wave energy conversion to mitigate coastal Erosion from hurricanes. J Mar Sci Eng 2022;10(2):143. https://www.mdpi.com/2077-1312/10/2/143.

[38] Ozkan Cigdem, Perez Kelsey, Mayo Talea. The impacts of wave energy conversion on coastal morphodynamics. Sci Total Environ 2020;712:136424. https://doi.org/10.1016/j.scitotenv.2019.136424.

[39] Ribeiro M, Taborda R, Cascalho J, Bosnic I, Oliveira A, Rodrigues A, et al. Grain size effects on suspended sediment concentration profiles under breaking waves. J Coast Res 2011:130–4. http://www.jstor.org/stable/26482147.

[40] Rodriguez-Delgado Cristobal, Bergillos Rafael J, Iglesias Gregorio. Dual wave farms for energy production and coastal protection under sea level rise. J Clean Prod 2019;222:364–72. https://doi.org/10.1016/j.jclepro.2019.03.058.

[41] Rodriguez-Delgado Cristobal, Bergillos Rafael J, Iglesias Gregorio. Dual wave farms and coastline dynamics: the role of inter-device spacing. Sci Total Environ 2019;646:1241–52. https://doi.org/10.1016/j.scitotenv.2018.07.110.

[42] Rodriguez-Delgado Cristobal, Bergillos Rafael J, Ortega-Sánchez Miguel, Iglesias Gregorio. Protection of gravel-dominated coasts through wave farms: layout and shoreline evolution. Sci Total Environ 2018;636:1541–52. https://doi.org/10.1016/j.scitotenv.2018.04.333.

[43] Rodriguez-Delgado Cristobal, Bergillos Rafael J, Ortega-Sánchez Miguel, Iglesias Gregorio. Wave farm effects on the coast: the alongshore position. Sci Total Environ 2018;640-641:1176–86. https://doi.org/10.1016/j.scitotenv.2018.05.281.

[44] Shadmani Alireza, Nikoo Mohammad Reza, Etri Talal, Gandomi Amir H. A multi-objective approach for location and layout optimization of wave energy converters. Appl Energy 2023;347:121397. https://doi.org/10.1016/j.apenergy.2023.121397.

[45] Sun Peidong, Bin Xu, Wang Jichao. Long-term trend analysis and wave energy assessment based on ERA5 wave reanalysis along the Chinese coastline. Appl Energy 2022;324:119709. https://doi.org/10.1016/j.apenergy.2022.119709.

[46] Trueworthy Ali, Gaebele Daniel, Jones Kristin, Hermanson Ian, Grear Molly. Wave energy in season: a comparative approach to feasibility of seasonal deployments for remote coastal communities. Appl Energy 2025;396:126206. https://doi.org/10.1016/j.apenergy.2025.126206.

[47] van Rijn, LC 1993. "Principles of sediment transport in rivers, estuaries and coastal seas." *Aqua Publications* The Netherlands.

[48] Veigas M, López M, Iglesias G. Assessing the optimal location for a shoreline wave energy converter. Appl Energy 2014;132:404–11. https://doi.org/10.1016/j.apenergy.2014.07.067.

[49] Williams Jon J, Esteves Luciana S. Guidance on setup, calibration, and validation of hydrodynamic, wave, and sediment models for shelf seas and estuaries. Adv Civ Eng 2017;2017:5251902. https://doi.org/10.1155/2017/5251902.

[50] Wimalaratna Yuhani Pamodha, Hassan Ateeb, Afrouzi Hadi Nabipour, Mehranzamir Kamyar, Ahmed Jubaer, Siddique Bazlul Mobin, et al. Comprehensive review on the feasibility of developing wave energy as a renewable energy resource in Australia. Cleaner Energy Syst 2022;3:100021. https://doi.org/10.1016/j.cles.2022.100021.